ISSN 0016-8521, Geotectonics, 2012, Vol. 46, No. 3, pp. 185–211. © Pleiades Publishing, Inc., 2012.
Original Russian Text © V.S. Burtman, 2012, published in Geotektonika, 2012, Vol. 46, No. 3, pp. 18–46.

Geodymanics of Tibet, Tarim, and the Tien Shan in the Late Cenozoic

V. S. Burtman

Geological Institute, Russian Academy of Sciences, Pyzhevskii per. 7, Moscow, 119017 Russia
e-mail: vburtman@gmail.com

Received August 29, 2011

Abstract—The tectonic and geodynamic consequences of the collision between Hindustan and Eurasia are considered in the paper. The tectonic evolution and deformation of Tibet and the Tien Shan in the Late Cenozoic is described on the basis of geological, geophysical, and geodetic data. The factual data and their interpretation, which shed light on the kinematics of the tectonic processes in the lithosphere and the geodynamics of the interaction between the Tien Shan, Tarim, and Tibet are discussed. A geodynamic model of their interaction is proposed.

DOI: 10.1134/S0016852112030028

INTRODUCTION

High Asia, Tarim, and the Tien Shan (Fig. 1) are key areas for solution of the problems pertaining to collision and within-plate geodynamics. Collision was caused by the convergence of continents during closure of oceanic basins. In the Tien Shan, the last oceanic basin was closed in the Carboniferous. In High Asia, such processes took place in Carboniferous, Triassic, Cretaceous, and Cenozoic [6]. The Hindustan–Eurasia collision took place when the Neotethys ocean was closed in Cenozoic.

The current paper discusses and interprets the data on the kinematics of tectonic processes in the lithosphere and the geodynamics of interaction between the Tien Shan, Tarim, and Tibet.

Research methods. The surface, crust, and mantle of the region under consideration have been studied with geological, geophysical, space, and on-land geodesy. The data on the lithology, stratigraphy, and magnetostratigraphy have made it possible to outline the stages of the tectonic process and estimate its activity at certain stages. The geochemistry of the igneous rocks provides insights into the processes within the crust and upper mantle. The results of geothermal research are used for verification of the geodynamic models.

Determining the relationships of geological bodies and morphostructures with faults using techniques of structural geology and estimating the age of displaced structural elements with the use of the radiocarbon method and cosmic isotopes provide an opportunity for timing of faults and assessment of their amplitudes. The sites that underwent rotation are revealed with the paleomagnetic method. The fission-track analysis of apatite is used for estimating the exhumation rate of the Paleozoic basement in the Cenozoic and calculation of the mountain-building and denudation rates. Palinologic studies are helpful for estimation of the mountain topography age. Recurrent measurements from satellites provide evidence for the distribution and rate of contemporary deformations.

Seismic profiling and gravity measurements allow to determine the position of the Moho boundary and within-crust discontinuities. The distribution of earthquake epicenters and solution of focal earthquake mechanisms show the activity of tectonic sutures and the stress field of the Earth's crust. Seismic tomography demonstrates the localization and dimensions of subducted slabs and the kinematics and size of convection cells in the upper mantle.

Tectonic flow plays a substantial role in the geodynamic processes discussed in this paper. Change of the body shape (deformation) in the Earth's crust is related to the destruction of a body (brittle failure) or proceeds without destruction (rheological, or rheid deformation). These are ductile and creep deformations, the intensity and rate of which depend on the Bingham and creep viscosity of rocks, respectively.

All solids undergo creep deformation under the effect of long-term stress below the yield strength of materials. The creep velocity of rocks is very high. It is estimated at 10^{12}–10^{22} P for various rocks, 10^{22}–10^{23} P for the Earth's crust as a whole, and 10^{19}–10^{26} P for the lithosphere [10]. Creep deformation is a result of rock flow caused by long-term stresses acting under the effect of gravity, mantle plumes, convective currents, indentors, compaction, and decompaction in the crust and below it. The creep deformation rate is extremely

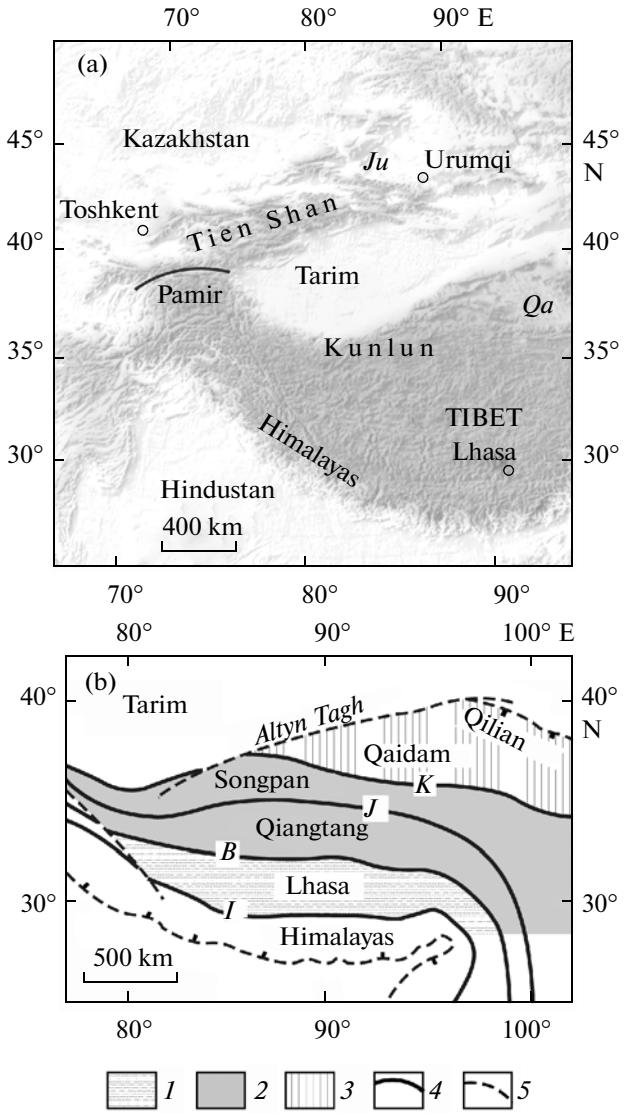

Fig. 1: (a) High Asia and Tien Shan and (b) geological–geographic provinces of Tibet. (*1*) Southern Tibet, (*2*) Central Tibet, (*3*) Northern Tibet; (*4*) oceanic sutures, (*5*) fault. Letters in panel (a): *Ju*, Junggar Basin; *Qa*, Qaidam; letters in panel (b): *B*, Bangong; *J*, Jinsha; *I*, Indus–Zangpo; *K*, Kunlun.

low, and its result becomes appreciable only if the process lasts for a long time.

Tectonic flow is a combination of rheological deformation and brittle failure with prevalence of the former. Brittle failure participates in tectonic flow in the form of faulting and cataclasis. The term *tectonic flow* may be applied to the entire crust, keeping in mind that the brittle failure develops in the upper crust and is very restricted or impossible in the lower crust. Many structural elements of collisional tectonics, including syntaxes and extrusions (protrusions), are results of tectonic flow.

The concept of flow in the Earth's crust, termed as sial or mass flow, facilitated the birth of collisional geodynamics developed by Argand [32]. The tectonic flow of the Earth's crust is often a subject (under various terms) of geodynamic interpretation [5, 14, 16, 27, 65].

COLLISION OF HINDUSTAN AND EURASIA

The time when Hindustan and Eurasia started to collide is widely discussed in the literature; it is determined taking into account the data concerned with movement of lithospheric plates, the formation of the Himalayas, the rise of Tibet, change in the sedimentation regime, etc. The onset of collision has been suggested as falling in the Late Cretaceous, 70–65 Ma ago [50, 94]; early Eocene, 55–45 Ma ago [52, 72]; and late Eocene, 35–34 Ma ago [30]. The results of recent studies provide evidence for a relatively young age of collision.

As follows from paleontological data [30, 88], the youngest marine sedimentary rocks in the Tethian Himalayas are late Priabonian in age (35–34 Ma). The oldest rocks containing clastic material derived from Hindustan and South Tibet are known as the upper Oligocene–lower Miocene Gangrinboche Conglomerate (Kailas, Qiuwu, Dazhuqu, and Luobusa formations), which is exposed on both sides of the oceanic Indus–Zangpo Suture. The Ar/Ar age of the tuffs intercalating within the conglomerates corresponds to the early Miocene (16.9 ± 0.2 and 20.1 ± 0.5 Ma) [30]. The rate of convergence of Hindustan and Eurasia decreased almost 1.5 times about 20 Ma ago [71]. Central and Southern Tibet was rising at approximately the same time.

The fold–thrust system of the Himalayas was formed as a result of collision. The fragments of the Himalayan metamorphic rocks appeared in the Himalayan Foredeep among the upper Oligocene sediments (Dagshai Formation) and became widespread in the Miocene Siwalik Formation. The results of paleoaltimetric study with application of the isotopic method [78] show that intense growth of the Himalayas started about 20 Ma ago.

The above data indicate that the collision between Hindustan and Eurasia began in the Oligocene–early Miocene, probably in the late Oligocene. This conclusion is consistent with the time of postcollision magmatism in Southern Tibet, which started 26 Ma ago [90, 100].

If the Hindustan–Eurasia collision began in the Oligocene, then it is necessary to understand the causes of the earlier events which gave grounds for the suggestion about the older age of the collision. Deceleration of convergence of the Indian and Eurasian plates 45–40 Ma ago [71], exhumation of eclogites, and metamorphism of the Himalayan rocks within the same time interval [93] can be mentioned among such

causes. To explain these and similar events, models of passing collision of Hindustan with intraoceanic island arc(s) that predated the Hindustan–Eurasia collision have been proposed [30, 50].

The formation of the Himalayan Fold–Thrust Belt was a consequence of the collision between Hindustan and Eurasia. As a result of deformation of the Earth's crust in the Himalayas and subduction of the Hindustan lithosphere beneath Tibet during the orogeny, the territory of the Hindustan continent became markedly reduced in area. Using the method of balanced sections, the shortening of the Himalayan Foldbelt in the process of orogeny is estimated at 200 to 470 km in Pakistan, 600–750 km in western Nepal, and 535–570 km in the eastern segment of the Himalayas [46, 48, 76, 93]. The pre-collision Hindustan continent is called Greater India. Dozens of reconstructions of Greater India have been proposed on the basis of paleomagnetic data, reconstruction of eastern Gondwana, calculation of underthrusting of Hindustan beneath Tibet, and other evidence and reasoning. The width of the part of Greater India which was deformed and subducted after collision is estimated at several hundreds of km to 2000 km. In the model based on seismic tomographic data [60, 99], the width of this part of Greater India is about 800 km and thus is comparable with the above values of transverse shortening of the deformed Himalayas.

TIBET

Contemporary Tibet consists of several sialic blocks, which were separated by oceanic basins in the geological past. The Qaidam Block together with the Kunlun and Qilianshan fold systems make up Northern Tibet Province (Fig. 1). The Songpan and Qiangtang blocks form Central Tibet Province, and the Lhasa Block is regarded as Southern Tibet Province. The high-mountain Tibet Plateau combines Central and Southern provinces (Central and Southern Tibet).

Deformation of Tibet

The contemporary deformation of Tibet is being studied with seismological methods and GPS. Earthquake epicenters occur throughout the territory of Tibet. Earthquakes no deeper than 15 km having shear-type source mechanism are predominant. Earthquakes with medium magnitude and hypocenters within the lithospheric mantle (70–113 km) happened in Southern Tibet and Himalayas. The mechanisms of these earthquakes indicate extension in the latitudinal direction [44, 70]. The density of earthquakes (number per area unit) in Tibet and Himalayas is much lower than in the northwestern Kunlun, Pamir, and Tien Shan (Fig. 2). The Qilianshan, with a high earthquake density, is the only exception.

The rate of current shortening of the territory between the Hindustan and Tarim–Alashan platforms has been calculated from GPS data along the profiles which cross Himalaya, Tibet, Kunlun, Qaidam, Qilianshan, and Altyn Tagh in the direction 20° NE (Fig. 3). Along profile *a*, the territory shortens with a rate of 34.6 ± 4.0 mm/yr; along profile *b*, 34.6 ± 3.0 mm/yr; along profile *c*, 33.6 ± 2.0 mm/yr; and along profile *d*, 28.0 ± 2.5 mm/yr [85, 99].

The GPS data also illustrate the internal deformation of Tibet. Central and Southern Tibet shorten in the meridional direction with a rate of ~10 mm/yr [98]. At present, the transverse shortening of Tibet is compensated by its longitudinal elongation. The westward elongation of Tibet is insignificant (2–3 mm/yr), whereas the eastward elongation reaches 20 mm/yr (Fig. 4). The elongation rate gradually increases from the northern and southern margins toward the axial zone which is situated at the boundary between Southern and Central Tibet (32° N). This rate distribution indicates that the deformation of Tibet is related to tectonic flow. The internal structure of the eastward flow in Southern Tibet is right-lateral and gives way to left-lateral flow in the north. The tectonic flow also includes offsets along strike-slip faults. The rate of the offset along the East Kunlun Fault is estimated at 4–10 mm/yr [44] or 8–11 mm/yr [98] and corresponds to the rate of the eastern component of tectonic flow.

Late Cenozoic deformation. According to the geological data, the transverse shortening and longitudinal elongation of Tibet occurred in the Late Cenozoic. The latitudinal thrust faults and folds in the Cenozoic rocks serve as a structural manifestation of the meridional shortening of the region. The transverse shortening of Southern Tibet is about 50 km [40]; the meridional shortening of Central Tibet is estimated at 260–280 km [48]; and the transverse shortening of Northern Tibet is ~200 km [84]. The above values are not results of direct measurements of deformation along the balanced geological sections or estimations of thrust amplitude. They are based on the offsets along the flank strike-slip faults, extrapolation of the current shortening in the geological past, and paleomagnetic data characterized by large uncertainty limits.

The longitudinal elongation of Tibet is estimated at 40 km [48] or 100–150 km [92] and compensates a significant part of the transverse shortening of Tibet in the Late Cenozoic. The intense longitudinal elongation of Tibet started in the Miocene about 18 Ma ago, intensified further in the Pliocene [94], and was accompanied by the formation of structural elements related to latitudinal extension, e.g., meridional grabens, normal faults, conjugate oblique strike-slip faults, etc. [92].

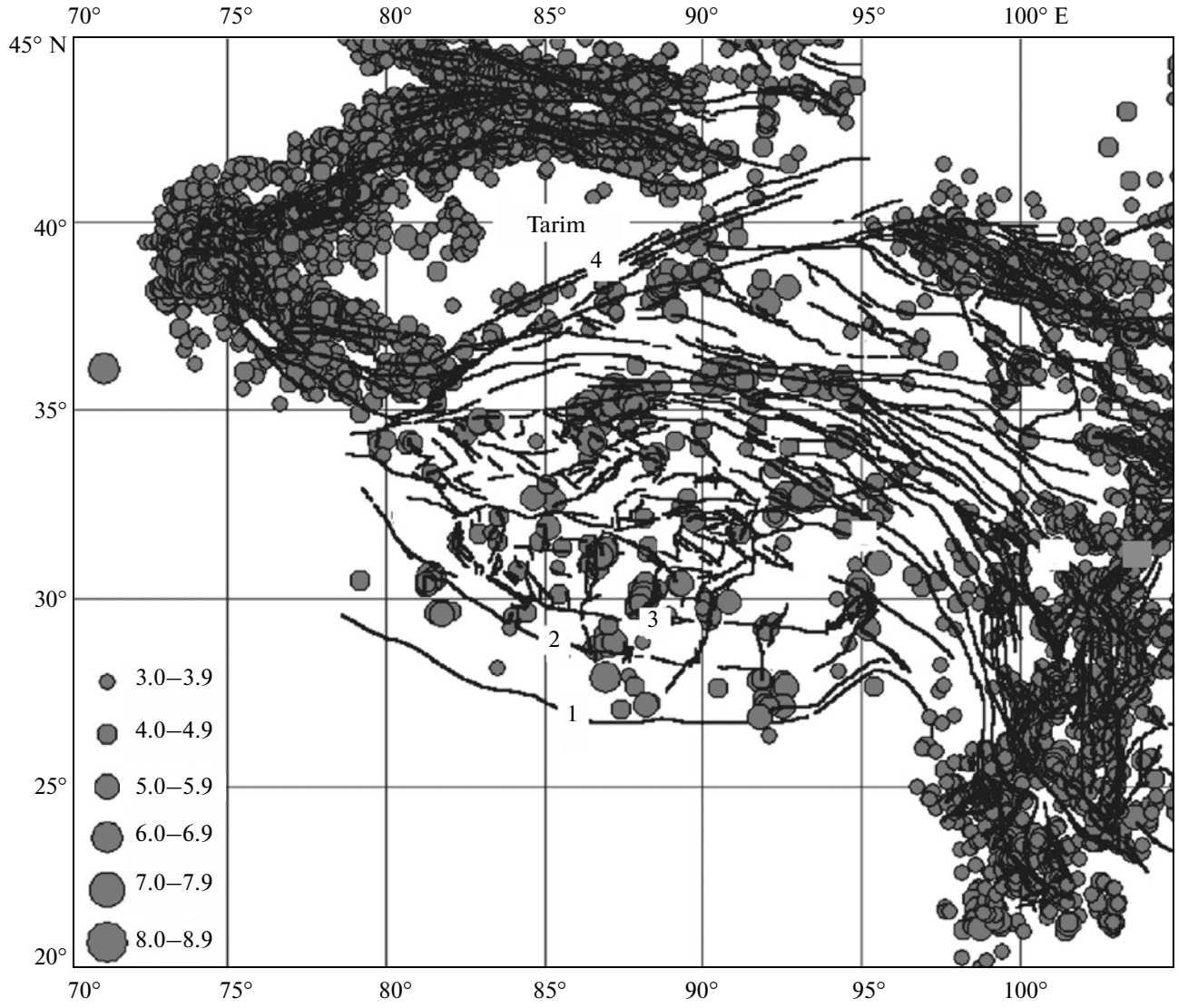

Fig. 2. Epicenters of earthquakes that occurred in Tibet and the adjacent territories since 1985, after [99]. Numerals in figure: 1, Main Boundary Thrust Fault of the Himalayas; 2, Main Central Fault of the Himalayas; 3, Indus–Zangpo Suture; 4, Altyn Tagh Fault.

As in the contemporary epoch, the longitudinal elongation of Tibet in the Late Cenozoic was caused by tectonic flow of the Earth's crust. The paleomagnetic data on the rocks of northern Tibet show that after the Oligocene sites of the province did not undergo appreciable lateral rotation relative to the reference paleomagnetic poles [51]. This implies that the tectonic flow of the Earth's crust was mainly laminar. Trails of horizontal rotation of several sites in the Miocene have been detected in the Qilianshan–Nanshan Fold System with numerous thrust and strike-slip faults.

Tectonic Boundaries of Tibet

The Indus–Zangpo Suture—a trail of the Neotethys ocean—is a boundary of Hindustan and the Himalayas with Tibet. This boundary is accompanied by a zone of thrust faults. The northern boundary of Tibet is two-step. The Eastern Kunlun mountain ranges separate the high-mountain plateau of Central and Southern Tibet (~5 km in height) from the Qaidam Plateau (~3 km in height). The mountain systems of Altyn Tagh, Nanshan, and Qilianshan separate Qaidam from the deserts of Tarim and Alashan Gobi (1–2 km in height). The mountain ridges at the boundaries of Tibet are distinguished by high seismicity related to strike-slip and thrust faulting.

The Altyn Tagh faults. The system of nearly parallel fractures of the Altyn Tagh Range taken together are called the Altyn-Tagh Fault, which extends in the northeastern direction for more than 1200 km. This fault separates the rigid Tarim Block from the

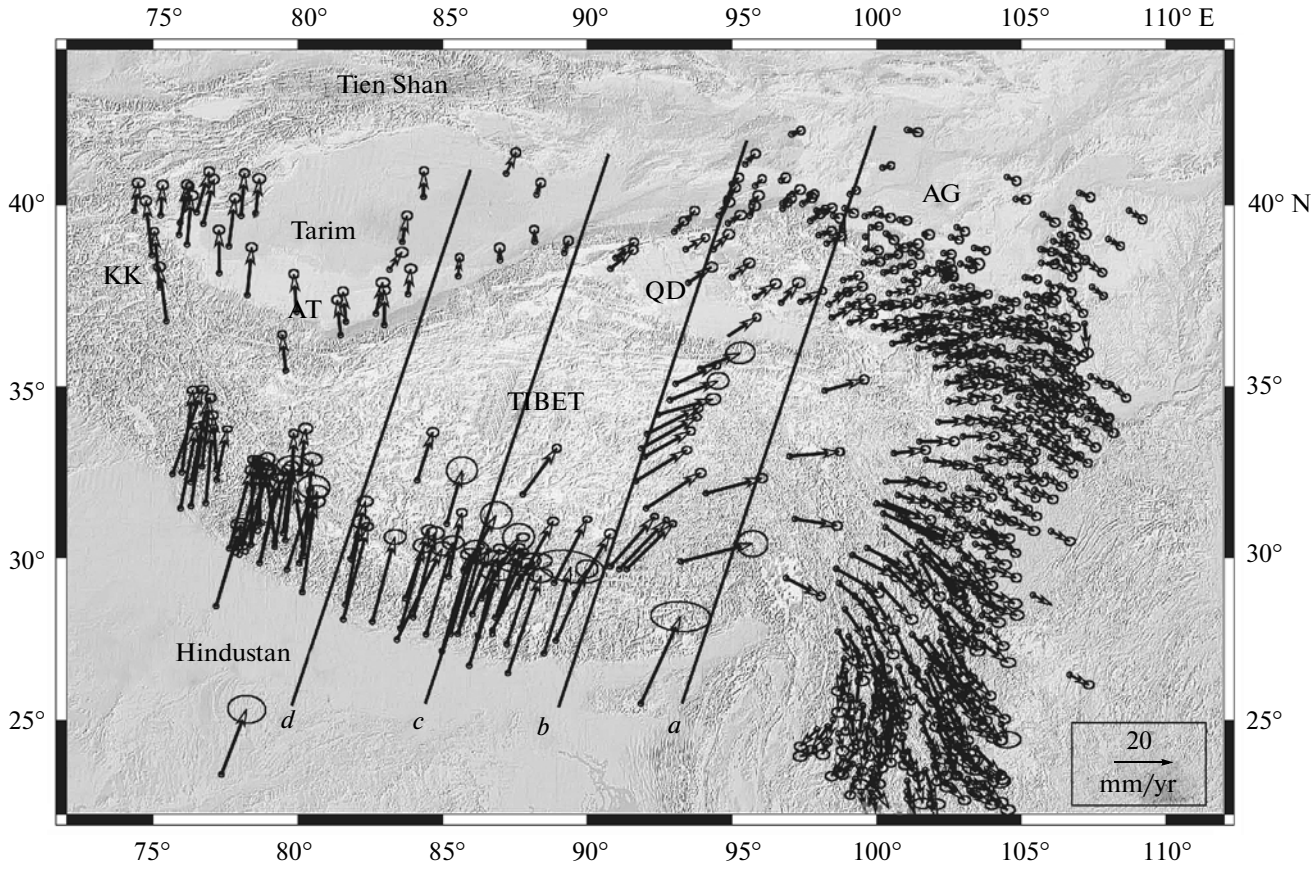

Fig. 3. Vectors of displacement rates of GPS stations relative to stable Eurasia, after [85, 99]. Ellipses indicate confidence interval of measurements. Abbreviations in figure: AG, Alashan Gobi; KK, Karakoram Range; QD, Qaidam.

deformed Northern Tibet. The latter includes a relatively rigid Qaidam Block. As follows from GPS data, the rate of current left-lateral offset along the middle segment of the Altyn Tagh Fault is 11.4 ± 2.6 mm/yr and decreases to 1 ± 2 mm/yr in the northeastern segment [97]. The total offset along the Altyn Tagh Fault after the middle Oligocene is estimated at 375 ± 25 km [96]. Thrust faults and folds of the Nanshan and Qilianshan, on the one hand, and the Western Kunlun and Northwestern Tibet, on the other hand, compensate the offset along the Altyn Tagh Strike-Slip Fault in the Cenozoic.

The average rates of displacements along the central segment of the Altyn Tagh Fault in the Holocene were estimated at 9.4 ± 0.9 and 13.7 ± 1.3 mm/yr from the offsets of morphostructures dated by the radiocarbon method. The average displacement rate over the middle Miocene–Holocene determined using various methods is ~10 mm/yr [47, 97]. The two-fold and three-fold higher slip rates in the Holocene are derived from the offsets of the river terraces and moraines dated by radiocarbon methods at the three sites in the central and eastern segments of the fault [84].

The Kunlun faults. The faults of the Eastern Kunlun, termed as the Eastern Kunlun or Kunlun Fault extends for 1600 km along the range bearing the same name. Five earthquakes with magnitudes above 7, which happened here over 100 years, were accompanied by left-lateral offsets of the landforms by 6–10 m [53]. The rate of the current offset along the Eastern Kunlun Fault is estimated at 4–10 mm/yr [44] or 8–11 mm/yr [98].

The isotopic age of the alluvial terraces displaced along the strike-slip fault in the late Pleistocene and Holocene has been determined and the average displacement rate calculated at 11.5 ± 2 mm/yr for the 600-km segment of the Eastern Kunlun Fault [84]. A series of pull-apart basins is localized along the Eastern Kunlun Fault Zone. The oldest sediments filling these basins are Pliocene in age [53]. This indicates that strike-slip offsets along the Eastern Kunlun Fault began in the Pliocene or late Miocene.

The strike-slip displacements along the northern boundary of Central Tibet were coeval to the thrusting of Central Tibet over Qaidam and Tarim or alternated with it. The ancient rocks of the Kunlun are thrust over Tertiary rocks of the Qaidam Basin along the fault sys-

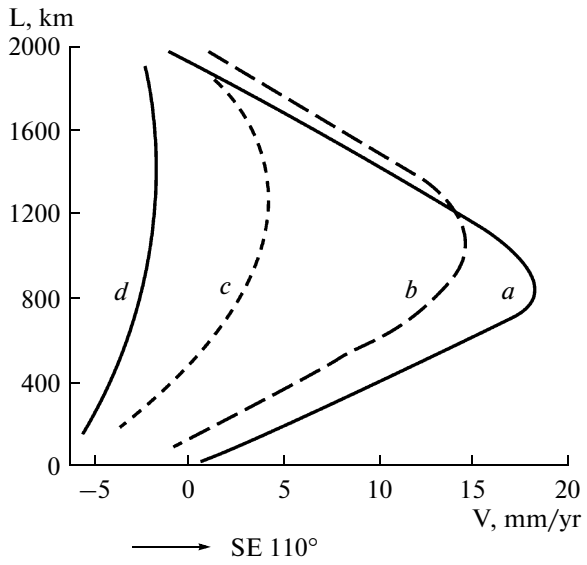

Fig. 4. Displacement rates of GPS stations toward 110° SE in profiles across the Himalayas and Tibet (Fig. 3, lines *a*–*d*). V, displacement rate, mm/yr; L, distance from the southern end of profile, km [99].

tems extending along the northern slope of the Eastern Kunlun (Qimen Tagh, etc.). In the west, thrust faults are conjugated with the Altyn Tagh Strike-Slip Fault or displaced along this fault. The estimate of thrust amplitude (270 km) is relied on the offsets along the Altyn Tagh Strike-Slip Fault [94]. The underthrusting of the Eurasian lithosphere beneath Tibet in the late Miocene and afterward is related to this thrust-fault zone [84].

In the Western Kunlun, high-mountain Tibet directly borders on the Tarim Basin. The ancient rocks of the Kunlun and Tibet are thrust northward over the Cenozoic rocks, the youngest of which are Pliocene in age. The amplitude of Cenozoic thrusting is estimated at 50–100 km [94]. The teleseismic data show that the Tarim lithosphere plunges beneath Tibet at an angle of ~45° [99]. According to the GPS data, in the Western Kunlun, Tarim thrusts under Tibet with a rate of 5–10 mm/yr [77].

The large Karakoram–Jali Strike-Slip Fault Zone extends near the boundary between Central and Southern Tibet. The right-lateral movement along this zone developed in the Holocene with a rate of 10 ± 6 mm/yr [33].

The data mentioned above show that the offsets along the boundary strike-slip faults occurred in the Holocene. Northern Tibet was displaced in the northeastern direction relative to the Tarim Block, while Central Tibet moved in the eastern direction relative to Northern and Southern Tibet. The Late Quaternary kinematics is consistent with the present-day regional kinematics established from GPS data.

Postcollision Magmatism in Central and Southern Tibet

After collision of Hindustan and Eurasia, magmatism remained active in Southern Tibet in the late Oligocene–Miocene and in Central Tibet in the Miocene to Quaternary. Trachyte, trachyandesite, trachybasalt, and other dikes (ultrapotassic alkaline rocks and high-K adakite igneous rocks typical to collision-related adakites) occur in Southern Tibet [90]. Many meridional dikes are associated with normal faults and grabens oriented in the same direction, indicating that injection of them was related to the longitudinal extension of Tibet. In Southern Tibet, adakites vary from 26 to 10 Ma in age and ultrapotassic rocks are dated at 25 to 8 Ma. The mantle-derived igneous rocks were contaminated by lower crustal material (adakites) or upper crustal material (ultrapotassic rocks) [90]. The volcanism was probably caused by continental subduction of the Hindustan lithosphere beneath the Tibetan crust.

A vast field of volcanic rocks pertaining to the high-K and partly adakitic group is located in the Songpan Block and northern Qiangtang Block of Central Tibet. The volcanic activity started 20 or 15 Ma ago, became widespread after 13 Ma, and continued into the Quaternary. Geochemical data provide evidence for contamination with lower crustal material. Volcanic activity in Central Tibet serves as evidence for the continental subduction of the Northern Tibetan and Tarim lithosphere beneath Central Tibet [54, 74].

The Earth's Crust and Upper Mantle of Tibet

The thickness of the Earth's crust in the southeastern Lhasa Block reaches 80 km. In the Qiangtang and Songpan blocks, it decreases northward to 65–60 km [60]. In Western Tibet, the crust thickness is 75–80 km [99] and reaches 90 km in the western Qiangtang Block [89]. In Northern Tibet, the Moho occurs at a depth of ~50 km [55].

The lower crust in the Lhasa Block, 15 km thick, is distinguished by high seismic wave velocity (7.2 km/s and higher) [48]. The seismic wave velocities in the uppermost mantle are high in the southern part of Tibet and lower in the north [84]. The high-velocity lower crust and upper mantle of Southern Tibet are interpreted as the Hindustan lithosphere.

The teleseismic section across the Tibetan Plateau (Fig. 5, line A–A) provides evidence for bilateral low-angle counter subduction of the Hindustan and Eurasian lithosphere beneath Central and Southern Tibet [60, 62]. The gently dipping slab of the Hindustan lithosphere underlines Southern Tibet. Near the Bangong Suture, the slab sharply bends and sinks vertically downward. In the section located to the west (Fig. 5, line B), the slab of the Hindustan lithosphere is traced to the Bangong Suture as well. In Western

Tibet (Fig. 5, line C–C), the Hindustan lithosphere is traced to the Jinsha Suture. The bottom of the slab gently plunges from a depth of 150 km near the Indus–Zangpo Suture for more than 200 km near the Bangong and Jinsha sutures. The Hindustan lithosphere has advanced beneath Tibet for 300–500 km from the Indus–Zangpo Suture. The bottom of the Eurasian lithosphere in this section gently plunges southward from the 120 to 140-km level. The high-velocity blocks are contained at various levels of the mantle in Southern and Central Tibet. They are interpreted as blocks of the cold lithosphere pertaining to the Indian Plate, which sank into the mantle as products of break-off and collapse of the slab during subduction of the Neotethian oceanic lithosphere and in the process of underthrusting of the Hindustan lithosphere beneath Tibet [48].

Tibet is characterized by the world's largest negative gravity anomaly, probably caused by heated and low-density mantle material. According to computation [35], high-mountain Tibet is isostatically compensated, so that the currently recorded uplift is driven by a tectonic (geodynamic) rather than isostatic force and Qaidam and Tarim are isostatically overcompensated.

Geodynamic Models

In 1922, E. Argand proposed a collision geodynamic model of the tectonic evolution of Asia in the Cenozoic [32]. This model endured transition from the geosynclinal hypothesis to the plate-tectonic paradigm and was updated and overgrown by variants and supplements. This model is the basis of most contemporary concepts concerning the Cenozoic geodynamics of Asia. The current geodynamic models involve the following processes in the formation of the Tibetan phenomenon.

The increase in thickness of the Earth's crust in Tibet is a result of deformation (stacking) and transverse shortening under the effect of the Hindustan indentor [68].

The results of such a process are strikingly expressed in the fold–nappe structure of the Himalayas. In Central and South Tibet, where Cenozoic rocks and denudation surfaces are deformed relatively weakly, this process did not play an appreciable role.

Squeezing-out (extrusion) of crustal material from the Himalayan–Tibetan domain proceeds in the eastern and, to a lesser extent, western directions under the effect of the Hindustan indentor on Tibet [48].

The squeezing-out of crustal masses is supported by GPS data (Fig. 3). The expansion of the Himalayan–Tibetan domain in the latitudinal direction in post-Oligocene time is consistent with this model. This process resulted in partial compensation and even in complete current compensation of the transverse shortening of Tibet.

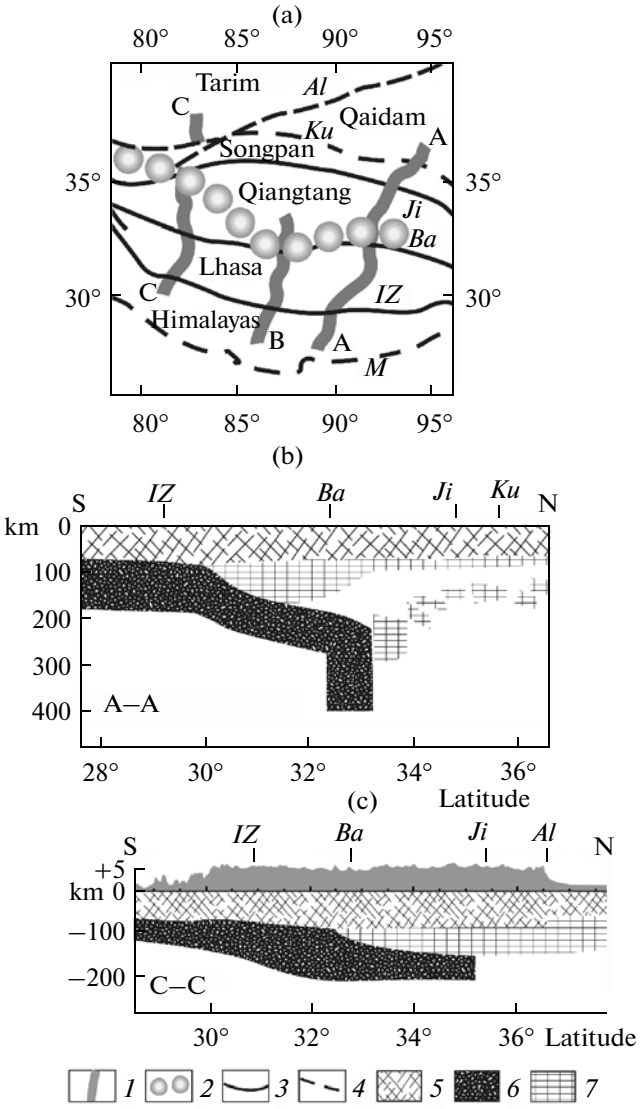

Fig. 5. Seismic sections across Tibet: (a) location of seismic lines, after [100]; interpretation of teleseismic data along lines (b) A–A, after [60] and (c) C–C, after [100]. The topography of Tibet with vertical exaggeration is shown above section C–C. Panel (a): (*1*) geophone bands; (*2*) northern boundary of the Hindustan lithosphere traced beneath Tibet (projection on the Earth's surface); (*3*) suture of oceanic basin; (*4*) fault. Panels (b) and (c): (*5*) Earth's crust, (*6*, *7*) lithospheric mantle: (*6*) Hindustan and (*7*) Eurasian. Structural elements (abbreviations in figure): *IZ*, Indus–Zangpo Suture; *Ba*, Bangong Suture; *Ji*, Jinsha Suture; *Al*, Altyn Tagh Fault; *M*, Main Boundary Thrust Fault of the Himalayas; *Ku*, East Kunlun and West Kunlun faults.

Subduction of the continental lithosphere operates at the Tarim–Tibet boundary and at the boundaries between some Tibetan sialic blocks [67, 89].

Underthrusting of Tarim beneath the margin of Tibet has been studied in the Western Kunlun and Qil-

ianshan. Subduction of the crust of Northern Tibet beneath Central Tibet in the Late Cenozoic is supported by manifestations of Pliocene–Quaternary magmatic activity in Central Tibet. Thrusting in the Eastern Kunlun fits the pattern of continental subduction. The results of teleseismic studies are in agreement with the subduction of Qaidam beneath Central Tibet. Subduction of the continental lithosphere at the boundary between Central and Southern Tibet is not yet reliably substantiated.

Underthrusting of the Hindustan crust beneath the Tibetan crust. According to the proposed models, after collision of continents, a slab of the Neotethian oceanic lithosphere was torn off and collapsed into the mantle, whereas the northern part of the Hindustan continental lithosphere was thrust beneath Tibet. Several variants of such a model have been proposed. Some models suggest that the Hindustan lithosphere was involved in underthrusting over the entire width of South and Central Tibet [75] or thrust only under Southern Tibet [45, 60]. In the latter case, the excess crustal thickness of Central Tibet is a result of subduction of the North Tibetan and Tarim lithosphere beneath Central Tibet. In terms of other models, the lower crust of Hindustan became detached from the mantle and the upper crust. The upper crust was being folded in the Himalayas, whereas the lower Hindustan crust intruded beneath the crust of Southern and Central Tibet and the Hindustan lithospheric mantle sank slantwise or vertically into the asthenosphere [48].

Conclusions. The regional geological features considered above, the manifestations of Late Cenozoic magmatism, the high-velocity mantle anomalies, as well as results of seismic sounding, profiling, and tomography are consistent with the assumption that the collision of Hindustan and Eurasia was followed by continental subduction of the Hindustan lithosphere beneath Tibet. Such subduction started in the Oligocene and was accompanied by modification of convective flows in the mantle under the effect of collision.

The transverse shortening of Central and South Tibet and squeezing-out of the Tibetan crust in the eastern and, to a lesser extent, western directions started in the Miocene. In addition to the near-meridional stresses induced by collision of continents, this process was controlled by the effect of gravity in highly rising Tibet. The crust of Tibet squeezed out into a "geodynamic refuge" [14] to the east and southeast of Tibet. In the late Miocene or Pliocene, the subduction of the lithosphere of Northern Tibet and Tarim beneath Central Tibet was switched on.

A conceptual model of the recent geodynamics of Tibet is shown in Fig. 6. According to this model, underthrusting of the Earth's crust or only the lower crust of Hindustan beneath the Tibetan crust occurred at a distance of 300–500 km from the Indus–Zangpo Suture. Having begun in Late Oligocene, underthrusting proceeded further at a rate of 10–20 mm/yr. This estimate is commensurable with the rate of underthrusting of Hindustan in the Holocene along the Main Boundary Thrust Fault of the Himalayas (21 ± 1.5 mm/yr) estimated from geological data [85].

TIEN SHAN

The Western, Central, Eastern, and Junggar geological and geographic provinces are distinguished in the Tien Shan (Fig. 7a). The extent of the Cenozoic Tien Shan Foldbelt is 2500 km. The belt consists of basement folds, which extend along the belt in the latitudinal and east-northeast directions. The length of the large folds is measured in hundreds of kilometers. Many folds are combined with the faults, which transform them into uni- or bilateral horst-anticlines, graben-synclines, and ramp-synclines. Anticlines and horst-anticlines are expressed in the topography as mountain ranges and synclines, graben-, and ramp-synclines are expressed as intermontane basins. The Cenozoic fold and faults of the Tien Shan are described in many books [18, 23, 24, 28, 29] and papers.

Most structural units of the Tien Shan are asymmetric. The asymmetry of the structural units determines their vergence. In the Central and Eastern Tien Shan, the structural elements are southward verging (toward Tarim). In the Junggar Tien Shan, the vergence of structural elements is directed toward the Junggar Basin [23, 31]. Two diagonal uplifts are important structural units of the Tien Shan (Fig. 7). The Karatau–Fergana Uplift (including the Greater Karatau, Talas, Atoinak, and Fergana mountain ranges) is associated with the right-lateral Talas–Fergana Strike-Slip Fault. The Borohoro–Bortoula Uplift (including the Borohoro, Irenhabirga, Keldyulu, Bortoula mountain ranges) is associated with the right-lateral Junggar Strike-Slip Fault. The combination of uplifts with right-lateral strike-slip faults indicates transpressional genesis of these oblique morphostructures.

Deformation of the Tien Shan

Current shortening of the Tien Shan. The territory of the Western and Central Tien Shan is covered by a dense network of GPS stations, which have monitored their geographic coordinates since 1992. The direction and rate of displacement of the GPS stations relative to stable North Eurasia are shown in Fig. 8. Most vectors are oriented in the northern direction. In the eastern part of the Central Tien Shan, the GPS stations mostly move in the northeastern direction. The displacement rate of the GPS stations in the Southern

Tien Shan is higher than in the north. The variable rate corresponds to the transverse shortening of the region due to its internal deformation. The convergence of Tarim with the Kazakh Platform, including transverse shortening of the Tien Shan, as well as over- and underthrusting at its boundary, is estimated at 20 ± 2 mm/yr [101]. The eastern component of the displacement rate of GPS stations increases in the east of the Central Tien Shan, indicating that the Tien Shan elongates eastward with a rate of ~5 mm/yr [12].

The displacement rate of the GPS stations sharply changes at the southern and northern boundaries of the Tien Shan, decreasing in the Tien Shan relative to Tarim and in Kazakhstan relative to the Tien Shan.

Compressive stresses in earthquake sources beneath the Tien Shan are oriented in the NNW direction [25]. The seismological data on earthquakes with magnitude 7 and higher recorded in the 20th century allowed calculation of the rate of meridional shortening of the Tien Shan [69]. The average rate of shortening of this mountain system is estimated at 7 ± 2 mm/yr. The shortening rates of the Western Tien Shan (18 ± 3 and 22 ± 4 mm/yr) coincide with the values obtained from cosmic geodesy.

How deep into history can the above data be extrapolated? An answer may be obtained from comparison of the shortening rates in the course of folding and thrusting with the displacement rate of the GPS stations located nearby. In the Central Tien Shan, numerous age determinations obtained with radiocarbon and luminescent methods for river terraces deformed by thrust faults in the Shu, Kochkor, Naryn, Atbashi, and Aksay basins are combined with the network of GPS stations. The displacement rate related to thrusting varies from 0.1 to 2.9 mm/yr. According to the available data, the Central Tien Shan between the Atbashi and Shu basins shortened over 140 thousand years with a rate of 11 mm/yr [86], and this estimate is consistent with the displacement rate of GPS stations. Thus, the cosmic geodetic data on current shortening of the Tien Shan may be extrapolated over the Holocene and late Pleistocene. It should be noted that the rate of current displacement along the oblique Talas–Fergana Strike-Slip Fault is much lower than the average rate of slipping along this fault in the Holocene [39].

Shortening of the Tien Shan in Late Cenozoic. Calculation of the rate of Cenozoic deformations meets difficulties because of their uncertain age, which is estimated from inferences of synchronism with deposition of specific sediments, growth of landforms, and other phenomena. Numerous publications are based on suggestions that the displacement rate of piedmont thrusting is related to the exhumation rate of the mountain range basement determined with fission-track dating of apatite [81]. The relationship between basement exhumation and displacement along faults remains unproved. It seems more probable that basement exhumation and mountain building are caused by the formation of a basement fold by rheological deformation; thrusting begins at the final stage of this process.

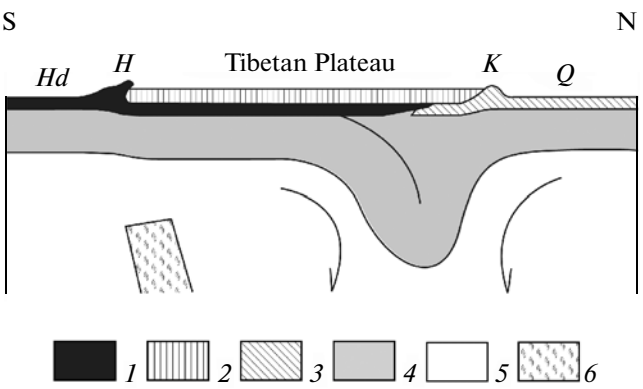

Fig. 6. Geodynamics of Tibet: a conceptual model. (*1–3*) Earth's crust: (*1*) Greater India, (*2*) Central and Southern Tibet, (*3*) Northern Tibet and Tarim; (*4*) continental lithospheric mantle; (*5*) asthenosphere (arrows indicate convection cells); (*6*) Tethian oceanic lithosphere. *H*, Himalayas; *Hd*, Hindustan; *K*, Kunlun; *Q*, Qaidam.

Shortening of the territory during orogeny is estimated on the basis of deformation of the preorogenic surface (peneplain) and Moho discontinuity.

Preorogenic surfaces and their deformation. The Late Paleozoic orogeny resulted in the formation of mountains in the territory of the Tien Shan. These mountains were not high, and destruction of them in the Late Permian led to peneplanation of the country. The weathering rind covered the peneplain in the Triassic and since then has mostly been eroded. In the Jurassic, Cretaceous, and Paleocene, a significant part of the peneplain was a slightly uplifted domain. The Late Cenozoic orogeny gave rise to its deformation and dismembering of the uplifted areas by linear erosion. As a result, the uplifted peneplain fragments were retained in mountains, whereas other fragments of the preorogenic surface were buried beneath younger sediments within depressions.

Various parts of the preorogenic surface differed in age before the onset of orogeny, and their fate in the process of mountain building was not similar. The peneplain worked out in the Permian underwent long-term but not deep planar denudation in the Mesozoic and Paleogene. Its depth did not reach the level of Paleozoic granites, so that the Cretaceous and Paleogene sediments are free of their fragments, which appeared only in the Miocene rocks. In the Mesozoic and Paleogene, a part of the older peneplain was overlapped by sediments and thus not involved in planar denudation. In the late Miocene to Holocene, frag-

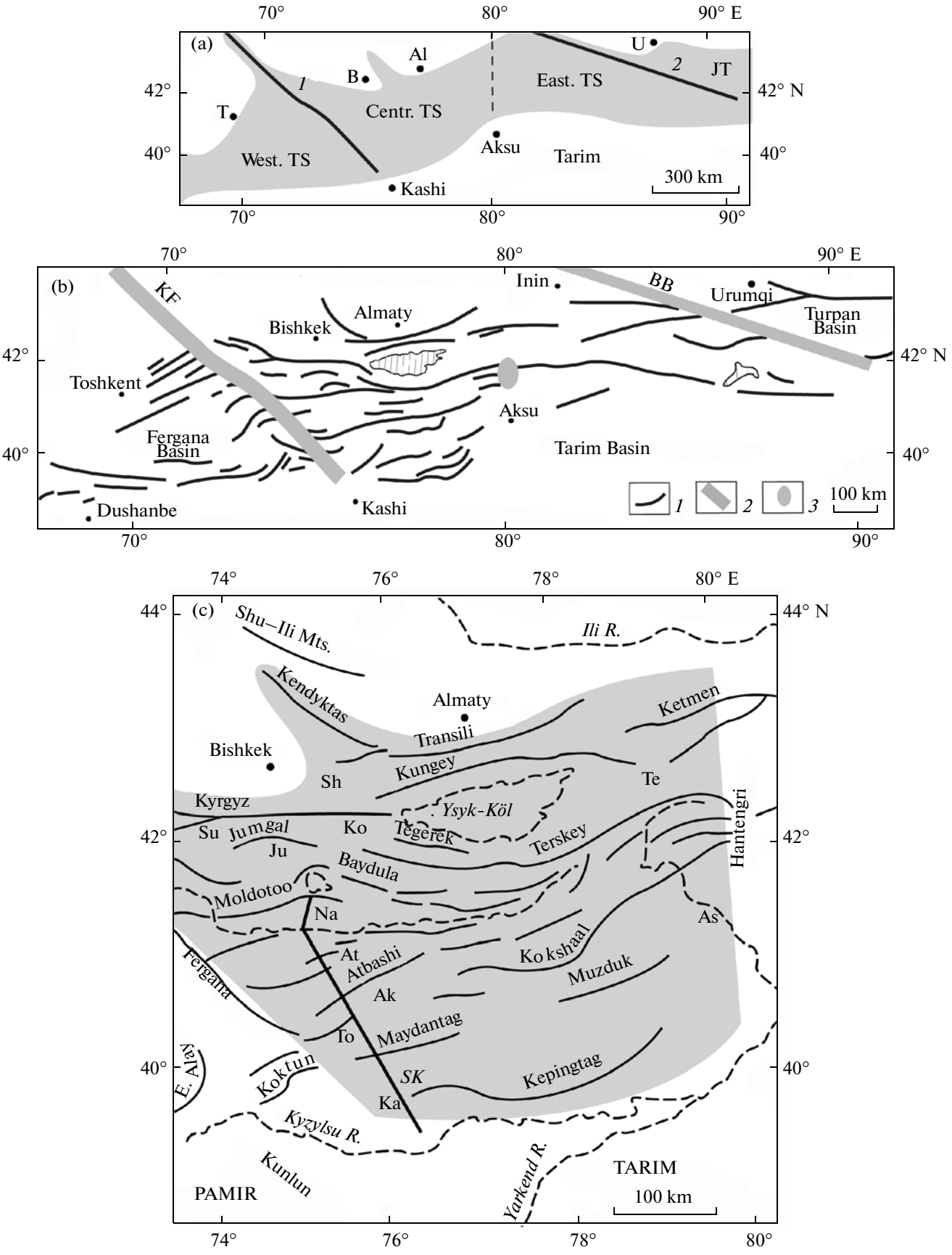
(a)
70°
80°
90° E
42°
42° N
40°
40°
Al
B
U
T
1
2
JT
East. TS
Centr. TS
West. TS
Aksu
Tarim
Kashi
300 km
(b)
KF
BB
Inin
Urumqi
Turpan Basin
Bishkek
Almaty
Toshkent
Aksu
Fergana Basin
Tarim Basin
Dushanbe
Kashi
1
2
3
100 km
(c)
74°
76°
78°
80° E
44°
44° N
42°
42°
40°
40°
Shu–Ili Mts.
Ili R.
Kendyktas
Almaty
Ketmen
Transili
Bishkek
Kungey
Sh
Te
Kyrgyz
Ysyk-Köl
Su
Jumgal
Ko
Tegerek
Terskey
Ju
Baydula
Hantengri
Moldotoo
Na
As
Fergana
At
Atbashi
Kokshaal
Muzduk
Ak
To
Maydantag
E. Alay
Koktun
SK
Kepingtag
Ka
Kyzylsu R.
Kunlun
Yarkend R.
PAMIR
TARIM
100 km

Fig. 7. Structural pattern and orography of the Tien Shan: (a) geological and geographic provinces. *1*, Talas–Fergana and *2*, Junggar strike-slip faults; Al, Almaty; B, Bishkek; T, Toshkent; U, Urumqi; TS, Tien Shan; JT, Junggar Tien Shan. (b) Late Cenozoic structural pattern of the Tien Shan. (*1*) Anticline and horst-anticline; (*2*) oblique transpressional uplifts (BB, Borohoro–Bortoula; KF, Karatau–Fergana); (*3*) Hantengri Uplift. (c) Orography of the Central Tien Shan. Mountain ranges are designated by solid lines, rivers and lakes by dashed lines. Intermontane basins and foredeeps (abbreviations in figure): Ak, Aksay; At, Atbashi; Ju, Jumgal; Ka, Kashi (Kashgar); Ko, Kochkor; Na, Naryn; Te, Tekes; To, Toyun; Su, Suusamyr; Sh, Shu; *SK*, Song-Köl–Kashi seismic line, see Fig. 11; the territory of the Central Tien-Shan is denoted by pattern.

ments of pre-Jurassic, pre-Cretaceous, and pre-Paleogene peneplain were uplifted together with overlying sediments, tilted or bent. Afterward, Mesozoic and Paleogene loose sediments were eliminated partly or completely by planar denudation. As a result, preorogenic denudation surfaces differing in age and retained beneath younger sediments were exhumed. Where fragments of sedimentary cover do not remain, it is impossible to estimate the age of the denudation surface. Geophysical methods also prove ineffective to detect the bottom of the Cenozoic molasse.

In the absence of angular unconformities in the Cretaceous–Paleogene section and conformable relationships between the Jurassic and Cretaceous beds in many areas, the Late Cenozoic fold structure can be described, relying on deformation of the Late Permian peneplain. The roof of Paleozoic rocks beneath the Mesozoic and Cenozoic fill of the intermontane basins is readily detected by geophysical methods. The reconstructed preorogenic surface inevitably consists of fragments differing in age. Some of them were affected by denudation over a long period up to the orogeny, whereas the others were formed much earlier, buried beneath the sedimentary cover, and exhumed in the Pliocene or Quaternary. The remnants of the Cretaceous–Paleogene sediments retained on the surface of highly uplifted peneplain fragments are limited in thickness. Therefore, the effect of the difference in the geological history of particular peneplain areas on the accuracy of reconstruction is not so great.

The preorogenic surface in the Central Tien Shan has been reconstructed along the meridian of 79° E from the Tarim Basin to the Kungey Range [28]. According to this reconstruction, folding resulted in shortening of this territory by 10 km, i.e., 6% of the initial length of the section. This and other calculations of shortening based on reconstruction of the deformed preorogenic denudation surface make it possible to estimate the effect of folding in the upper crust (Table 1, rows 1 and 2). The calculations take little account of the shortening of the Earth's surface related to thrusting because in most geological sections used for calculations, the faults were interpreted as steep normal or reverse disturbances.

Topography of the Moho discontinuity and deformation of the fold system. The relationships between pre- and postorogenic volumes of the Earth's crust or corresponding areas in cross sections display its *full deformation*, which includes ductile deformation in the upper crust, thrusting, and tectonic flow in the crust as a whole. The full deformation of the Earth's crust in the Tien Shan with retention of its volume calculated on the basis of topography of the Moho surface is given in Table 1. The authors of the calculations used various maps of the Moho surface, different thickness of the initial (preorogenic) crust, and different algorithms of computation. With allowance for these differences, the resultant values of full deformation of the Earth's crust in the Tien Shan are commensurable.

The Late Cenozoic deformation of the Tien Shan led to shortening of the fold system by 100 km if the thickness of the preorogenic crust was 40–42 km or 200 km if this thickness was 35 km. The average rate of shortening is 4 or 8 mm/yr. The transverse shortening decreases eastward, but the ratio of this value to the initial length of the section changes little because the width of the fold system also diminishes in the same direction.

Comparison of the data on folding and full deformation shows that faulting in the upper crust is more efficient than ductile deformation. The full transverse shortening of the Tien Shan, including both ductile deformation and faulting, is 2–6 times greater than shortening related to the effect of Cenozoic folding established at the surface.

Orogenic History of the Tien Shan

In the course of orogeny, its intensity was progressively increasing, whereas the duration of orogenic stages recognized in its history became shorter (Fig. 9).

Origination of orogeny (Oligocene–Miocene). The stage of embryonal orogeny lasted for ~15 Ma from 25–26 to 8–11 Ma. Red sandstone, siltstone, gravelstone, and fine-pebble conglomerate with clay and gypsum interlayers occupy the upper part of the Kyrgyz Complex of red beds. The structure of the stratigraphic sections and their thickness (100–1500 m) are variable between basins. In the Fergana, these rocks are referred to the Maylisay, Obchak, and other formations; in the Central Tien Shan basins, to the Kökömeren, Kyrgyz, and other formations. The clastic rocks are poorly sorted and are related to local provenances; the sediments become coarser upsection. Most rocks are proluvial sediments of intermittent streams and fans; fluvial and lacustrine sediments are also noted.

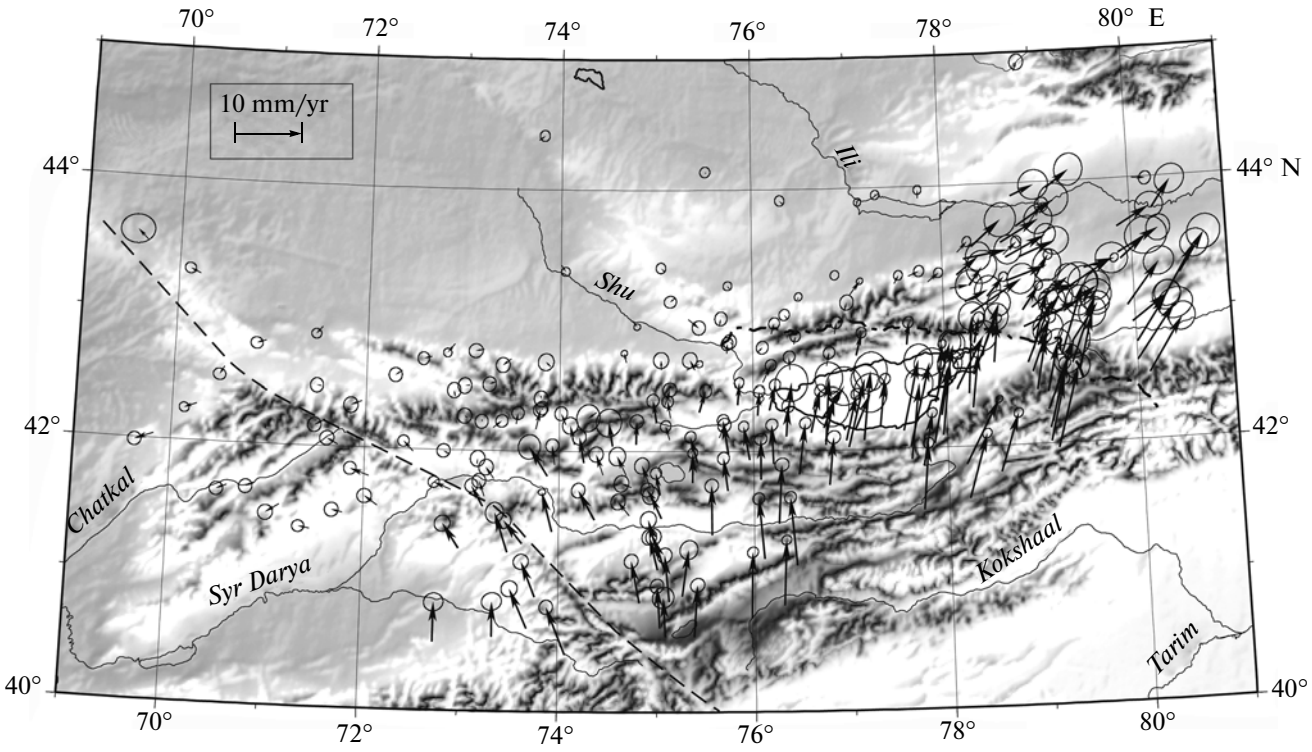

Fig. 8. Vectors of displacement rates of GPS stations in the Western and Central Tien Shan relative to stable Eurasia over 1995–2005, after [11]. Ellipses indicate the confidence interval of measurements. The Talas–Fergana Fault is shown by a dashed line.

Oligocene and Miocene fossil turtles, teeth of Miocene giraffe, and bones of Miocene and early Pliocene vertebrata have been found in these sediments. Early and middle Miocene ostracods are contained in the lacustrine sediments. The palynological complexes indicate the late Oligocene–late Miocene age. The magnetostratigraphic data show that the upper boundary of the late Miocene Kyrgyz red beds corresponds to the level of 8–9 Ma [1, 36].

The rate of sedimentation in the inner depressions of this stage was low (up to 60 m/Ma). In the outer basins, the rate is much higher. For example, in the Kuchar Basin at the margin of Tarim, the sedimentation rate between 17 and 16 Ma increased from 70 to 130 m/Ma [58]. In the Kashi Basin at the margin of Tarim, the sedimentation rate between 15 and 8 Ma increased from 80 to 400 m/Ma [57]. At the southern margin of the Junggar Basin the sedimentation rate between 16 and 10 Ma was 180 m/Ma [41].

The palynological spectra in the sediments of this epoch do not reveal staged mountain vegetation. In Oligocene and Miocene, the Tien Shan was a hilly plain with steppe vegetation and foliage forests [9]. The depth of erosion in Oligocene and Miocene is estimated at 300–600 m. The valleys were depocenters of clastic sediments and hosted the lakes with evaporites. The Miocene salt-bearing sediments are retained in most intermontane basins of the Western and Central Tien Shan.

The fission-track data on the rocks of the Paleozoic basement in the contemporary Kendyktas and Kungey ranges, as well as in some ranges of the Eastern Tien Shan, indicate a low rate of basement exhumation in the Oligocene and Miocene measured as 40–50 m/Ma [49]. Deep basins were formed at that time in the Muzduk and the eastern part of the Kyrgyz Ranges [80]. This implies that the hilly topography at the stage of embryonal orogeny did not fit the future mountain topography of this region.

The inner and outer depocenters that arose in the Tien Shan at this stage were separated by low drainage divides. The formation of these slowly developing synsedimentation morphostructures is a result of creep deformation of the Earth's crust, which developed synchronously with the onset of collision between Hindustan and Eurasia.

Early Orogeny (late Miocene–middle Pliocene). This stage lasted for 5–8 Ma from 8–11 to 2–3 Ma ago. The sediments of this age make up the lower part of the Tien Shan Orogenic Complex. The composition of the rocks is close to that of the Kyrgyz Complex, but the contribution of conglomerate increases; the sorting and roundness of the fragments is better. The rocks are colored in pale yellow, green, and gray tints. The

Table 1. Horizontal shortening of the Tien Shan in the meridional direction during the Late Cenozoic orogeny

No.	Meridian:	70°	71°	73°	74°	76°	78°	79°	81°	84°	85°	86°	Source
1	Fold deformation, %	7	5	5	–	4	–	>6	–	–	–	–	[28]
2	Fold deformation, %	4	–	12	12	9	–	–	–	–	–	–	[21]
3	Full deformation, %**	–	–	–	–	21	23	25	–	–	–	–	[27]
4	Full deformation, km*	–	–	–	–	251	258	–	215	141	154	95	[34]
5	"km***	–	–	–	–	96	107	–	74	54	66	38	"
6	Full deformation, %*	–	–	–	–	40	40	–	45	40	40	25	"
7	"%***	–	–	–	–	20	20	–	23	20	20	13	"
8	Full deformation, %**	15	21	23	25	17	18	16	–	–	–	–	[21]
9	Full deformation, km**	90	110	105	110	75	80	70	–	–	–	–	"

Notes: Fold and full deformations are values of shortening of the Tien Shan measured in kilometers and percents relative to the initial (preorogenic) length of the section. The full deformation has been determined using the maps of the Moho surface: *3* [27], *4–7* [66], and *8*, *9* [13]. Initial (preorogenic) thickness of the Earth's crust: * 35 km, ** 40 km, *** 42 km.

sections are characterized by transgressive succession of beds; large sedimentation rhythms are outlined in some sections. In Fergana, these sediments belong to the Akchop and other formations; in the Central Tien Shan, these are the Djuanarik, Ysyk-Kol, and other formations. The thickness of alluvial, proluvial, and lacustrine sediments in the basins of the Central Tien Shan is 2–3 km and greater. At the foothills of the Junggar Tien Shan, the upper part of the Taxihe Formation and the Sushanzi Formation correspond to the lower part of the Tien Shan Orogenic Complex. The bottom of this sequence is dated at 6 or 7 Ma depending on the correlation with the paleomagnetic scale and the roof is dated at 2.58 Ma [82, 83].

Bones and teeth of the late Miocene–Pliocene mammals, middle Pliocene turtles, and teeth belonging to the late Pliocene elephants are noted among the fossils. Early and late Pliocene gastropods, middle and late Pliocene mollusks, and Miocene fishes and insects have been found in the sediments of this stage. The palynological complexes are Pliocene in age.

According to the results of fission-track dating [37, 80], the fast exhumation of the Paleozoic basement of the future mountain ranges in the Central and Eastern Tien Shan started 10–12 Ma ago. The exhumation rate was variable; the rate of about 300 m/Ma was predominant. Sedimentation and denudation rates increased by an order of magnitude. In the valleys of the Central Tien Shan, the sedimentation rate reached 500–600 m/Ma [42] and 700–800 m/Ma in the Kashi Basin of Tarim [57]. These data provide evidence for significant intensification of erosion and activation of orogeny in the Tien Shan 10–7 Ma ago.

Transverse shortening of the Tien Shan at that time was related to the formation of large basement folds—mountain ranges and intermontane basins, the orographic pattern of which was close to the recent pattern. The topography was low-to-medium mountainous. The Earth's crust underwent ductile deformation. Faulting was probable, but its role remains ambiguous. The longitudinal expansion (elongation) of the Tien Shan by means of tectonic flow began at this stage.

Medium orogeny (middle Pliocene–middle Pleistocene). This stage lasted for 2.0–2.5 Ma from 2–3 to 0.5–0.6 Ma ago. The upper part of the Tien Shan Orogenic Complex was formed during this stage (conglomerate–breccia, boulder and pebble conglomerates, gravel, and pudding of proluvial and alluvial origins). These clastic rocks belong to the Sharpyldag Formation and its counterparts: the Ispisara Forma-

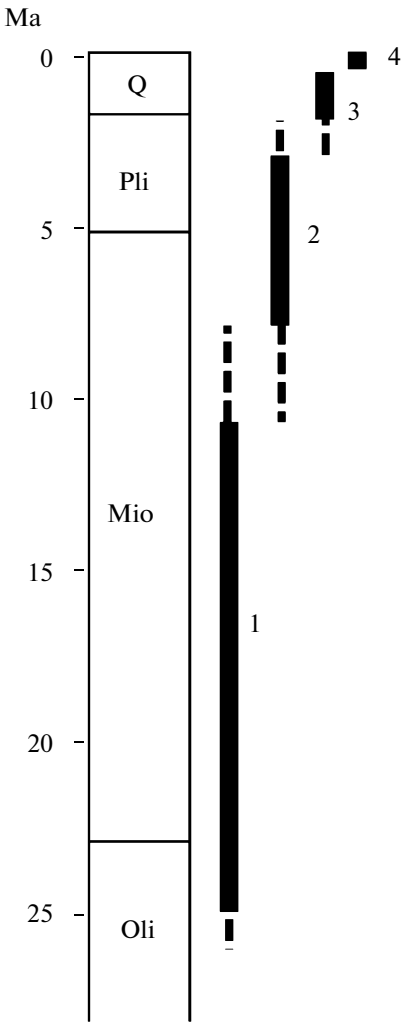

Fig. 9. Orogenic stages in the Tien Shan: 1, embryonal; 2, early; 3, medium; 4, late; Oli, Oligocene; Mio, Miocene; Pli, Pliocene; Q, Pleistocene and Holocene.

tion in Fegana Ulahol ad Horgos formations in the Central Tien Shan, and the Xiyu Formation in the foredeeps of the Central and Junggar Tien Shan. The fragment size increases upsection; some sections reveal a rhythmic structure. The thickness of sediments in the inner parts of the basins is measured in hundreds of meters. In the Shu and Ysyk-Kol basins, the thickness exceeds 1000 m and reaches 1700 m in the foredeep of the Borohoro Range in the Junggar Tien Shan.

The sediments contain bone remains of the middle–late Pliocene and Early Pleistocene mammals; Pliocene and Quaternary mollusca have been identified from lacustrine interlayers. According to magnetostratigraphic data, the bottom of the Sharpyldag Formation in the Shu Basin corresponds to the level of 3 Ma [36]. The bottom of the Xiyu Formation at the margin of the Junggar Basin is dated at 2.58 Ma [83]. In the upper part of the section in the Ysyk-Kol Basin, the age of rocks was determined at 570 ± 63 ka using the thermoluminescent method [2]. The deposition of the Sharpyldag Conglomerate and their analogues completed 600–500 ka ago in the middle Pleistocene (early Neopleistocene according to the scale of the Russian Stratigraphic Commission).

During the medium orogenic stage, the high-mountain topography of the Tien Shan was formed. Study of the spores and pollen from the sediments in the northern part of the Central Tien Shan has shown that the staged vegetation (up to Alpine meadows with Arctic flora) developed in the Pliocene [9]. The orographic pattern of the territory was complicated due to subdivision of the basins by inner ridges. As follows from the fission-track dating, the exhumation rate of the Paleozoic basement in the Kyrgyz Range (Ala-Archa Valley) increased ~3 Ma ago from 100–300 to 400–800 m/Ma [37]. The stage is characterized by a high sedimentation rate. In the Kashi Basin, it was estimated at 500–800 m/Ma [57].

The Sharpyldag Conglomerate and its counterparts make up the upper part of the Cenozoic section of the Tien Shan, where angular unconformities are rare local and poorly developed exceptions. The Earth's crust underwent ductile deformation at this stage. Transverse shortening of the region and its longitudinal expansion by means of tectonic flow continued. The pre-Pleistocene tectonic deformations bore synsedimentation character and were displayed in variable thickness and composition of sediments. The rheological deformation, which dominated in the upper crust earlier, gave way to brittle failure with rejuvenation of older faults and origination of new fractures.

Late orogeny (middle Pleistocene–Holocene). The duration of this stage is 500–600 ka. The deposits of river terraces and fans, moraines, and other sediments overlie older rocks with angular or stratigraphic unconformity. They mostly fill erosion valleys, which cut down the Sharpyldag and other older rocks. Middle Pleistocene fossils have been identified from the oldest sediments formed during this stage.

The high-mountain topography was affected by intense linear erosion. The history of the morphostructures in the Tien Shan was deduced from the staged structure of the river terraces and their relationships with alluvial and glacial sediments [28]. The retained terraces were formed in the Quaternary. The bones of mammals similar to the middle Pleistocene Tiraspol and Khazar faunal complexes of Europe have been found in the Western and Central Tien Shan, where they occur on the high and middle terraces of the Shu and Syr Darya rivers. Late Paleolithic tools and the bones of late Pleistocene vertebrata occur on the lower terraces. According to the calculations of A.K. Trofimov and O.K. Chediya based on terrace lev-

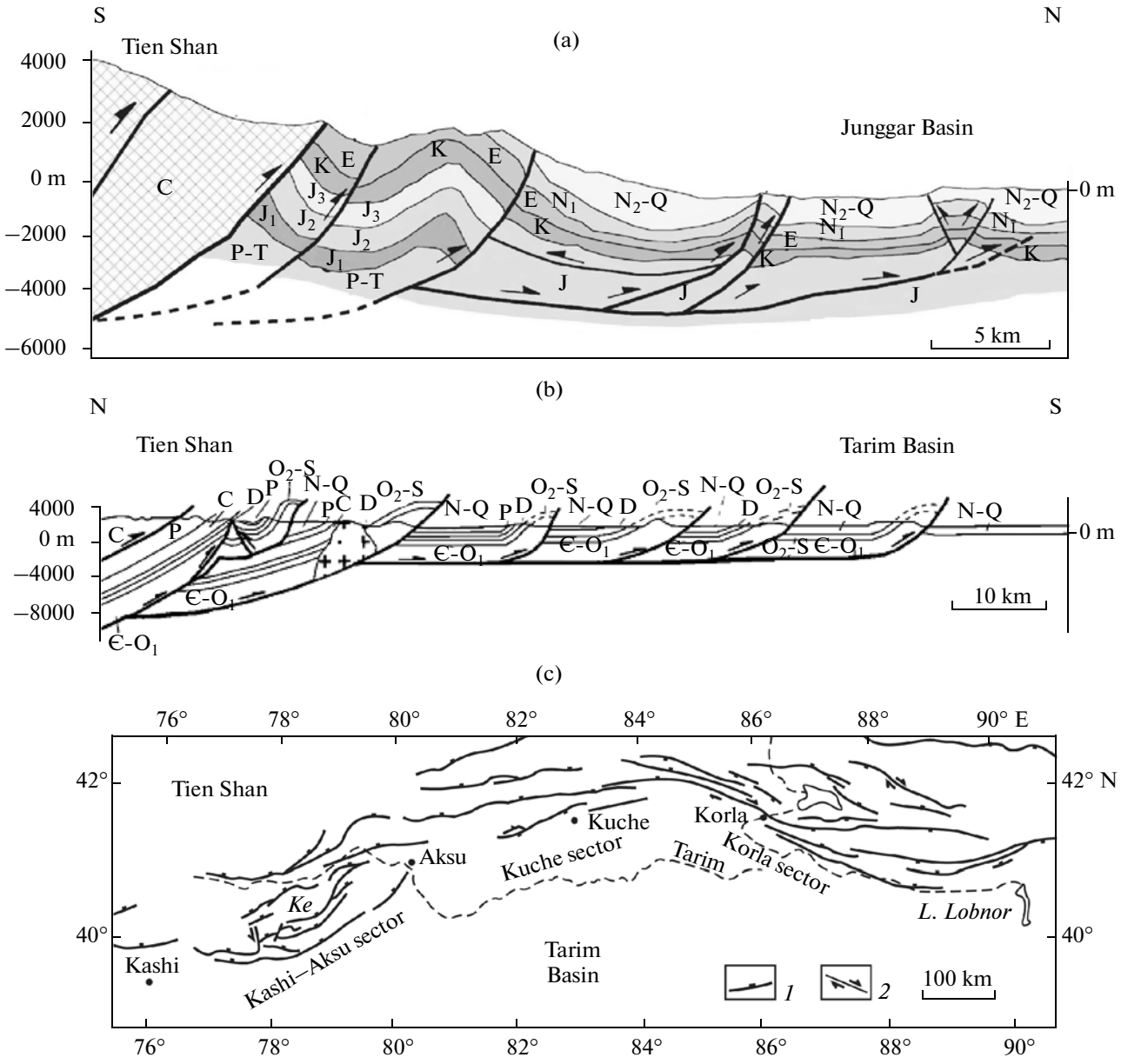

Fig. 10. Deformations at boundaries of the Tien Shan: (a) deformations at the Tien Shan–Junggar Basin boundary in geological section along meridian of 86° E, after [54]; (b) deformations at the Tien Shan–Tarim Basin boundary in geological section across the Keping Zone of dislocations (Fig. 10c, *Ke*) in the Kashi–Aksu sector, after [95]; (c) thrust and strike-slip faults at the Tien Shan–Tarim boundary [95]. (*1*)Thrust and (*2*) strike-slip faults; *Ke*, Keping Zone of dislocations.

els, the mountain ranges grew during this epoch with a rate reaching 4 km/Ma [17]. The intensity of erosion in the mountains was very high. The linear erosion rate in the Pleistocene and Holocene is estimated at 800–1000 m/Ma, on average [15].

The average rate of transverse shortening of the region was higher than 11 mm/yr and at present has reached 20 mm/yr; the rate of longitudinal elongation in the eastern direction has reached 5 mm/yr. The newly formed and older structural elements and landforms underwent intense faulting and ductile deformation.

The high-mountain topography of the Tien Shan was created in the Pliocene. Afterwards, its retention was maintained by rise of the mountain range basement and the steady balance between the rates of rise and denudation. Under such conditions, the rise amplitude of the mountain range basement as a result of orogeny can approximately be estimated by summing up the height of the present-day range and the magnitude of exhumation (approach to the surface) of

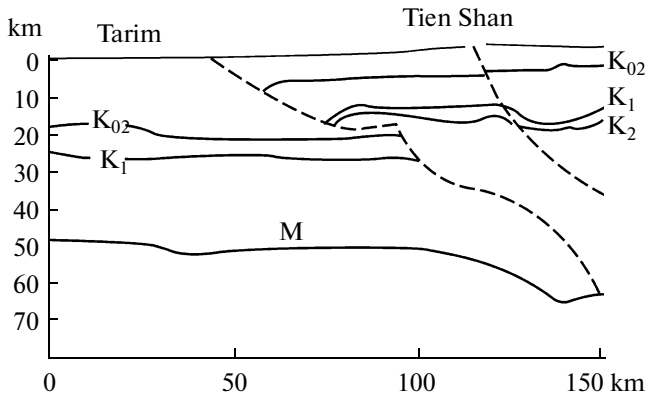

Fig. 11. Tectonic interpretation of the southern part of the reflection CDP seismic section along the Song-Köl–Kashi line, after [19]. The layer between K_{02} and K_1 reflectors occurs at the base of the upper crust; the layer between reflectors K_1 and K_2 (waveguide) has a low viscosity; M is the Moho boundary. The boundaries interpreted as faults are shown by dashed lines. The distance from the southern end of the section is noted at the horizontal axis. See Fig. 7 for the seismic line location.

its Paleozoic basement. As follows from fission-track timing, since the late Miocene, the basement of the Kendyktas, Kyrgyz, and Kungey ranges has been exhumed for 2–3 km; the average height of these ranges is 4.0–4.5 km. Thus, the basement of these ranges has been raised 6–8 km.

Tectonic Boundaries of the Tien Shan

The Tien Shan regions bounding about the young Kazakh and the ancient Tarim platforms are distinguished by high seismicity. The magnitude of strong earthquakes therein exceeded 8.0.

Boundary between the Tien Shan and the Kazakh Platform. The boundary with the Kazakh Platform is uneven. The branches of the Tien Shan mountain country (Karatau, Shu–Ili Mts.) are deeply embayed into the platform. The Shu and Junggar basins overlapping the platform margin were depocenters for the sediments supplied from the Tien Shan for a long time. Northward verging thrust faults are widespread at the northern boundary of the Tien Shan. This is a boundary between secondary lithospheric plates, which is forming now.

As follows from the GPS data, mobility of the territory markedly changes at the boundary of the Tien Shan with the Kazakh Platform. The marginal mountain ranges of the Tien Shan are currently thrusting over the outer basins: the Kyrgyz Range over the Shu Basin with a rate of 1.4–2.9 mm/yr [11] or 6.1 ± 0.8 mm/yr [91]; the Transili Range over the Ili Basin with a rate lower than 5 mm/yr [101] or 10.1 ± 0.4 mm/yr [91]. The relatively high rates of overthrusting published in [91] include part of the internal deformation of the Tien Shan. According to [91], the Ketmen Range is thrusting over the Ili Basin with a rate of 3.9 ± 0.9 mm/yr and the Irenhabirga Range is overlapping the Junggar Basin with a rate of 4.0 ± 1.4 mm/yr [91].

A system of thrust and strike-slip faults occurs on the northern slope and at the foothills of the Kyrgyz Range. The boundary zone has been shortened for 11 km as a result of folding and thrusting [36]. A zone of steep thrust faults is traced along the boundary between the Junggar Tien Shan and the Junggar Basin. The Mesozoic and Cenozoic rocks are folded and thrust in front of the boundary thrust faults. These dislocations are interpreted in terms of thin-skinned tectonics (Fig. 10); a detachment is inferred within the Lower Jurassic rocks. In the piedmont zone of the Junggar Tien Shan (Irenhabirga Range) 50–60 km wide, shortening of the surface in the course of deformation is estimated at 8–35 km. In the inner zone (near mountains), folding developed in the late Miocene to late Pleistocene, whereas in the outer zone, from late Pleistocene to the present time. The reduced thickness of Miocene sediments in the cores of anticlines indicates that they grew synchronously with sedimentation [34].

Boundary between the Tien Shan and the Tarim Platform. The Cenozoic orogeny of the Tien Shan spread beyond the Paleozoic fold region over the marginal part of the ancient Tarim Platform. The foredeeps at the margin of the Tarim Massif served as the outer depocenters for the Central and Eastern Tien Shan. The sediments filling the foredeeps are deformed. The Tarim margin is regarded as a zone of thin-skinned tectonics [80, 95].

In the Kashi Basin, the Mesozoic and Cenozoic sediments were deformed in folds. Anticlines are complicated by longitudinal thrust faults. Magnetostratigraphy of the Pliocene and Pleistocene sediments in the anticlines of the northern Kashi Basin shows that these folds started to grow 1.4–1.2 Ma ago [43]. The deformations presumably propagate down to the detachment related to the Miocene gypsum unit. This suggestion is supported by the seismic data, which do not reveal folding below a reflector detected at a depth of 6.2–6.5 km. The northern boundary of the Kashi Basin is complicated by a steep thrust fault. The Paleozoic rocks of the Tien Shan are thrust over Miocene and Pliocene–Pleistocene sediments filling the basin.

The eastern part of the Kashi–Aksu sector is occupied by the Keping area of deformation (Fig. 10, *Ke*), which is situated in the northern part of the Bachui Uplift of the Tarim Platform, where only ~1000 m of the Cenozoic sediments have been deposited instead of the sixfold thicker coeval sediments in the adjacent Kashi and Kuche basins. The Keping deformations are expressed in the arcuate system of steep thrust and reverse faults along with accompanying homoclines,

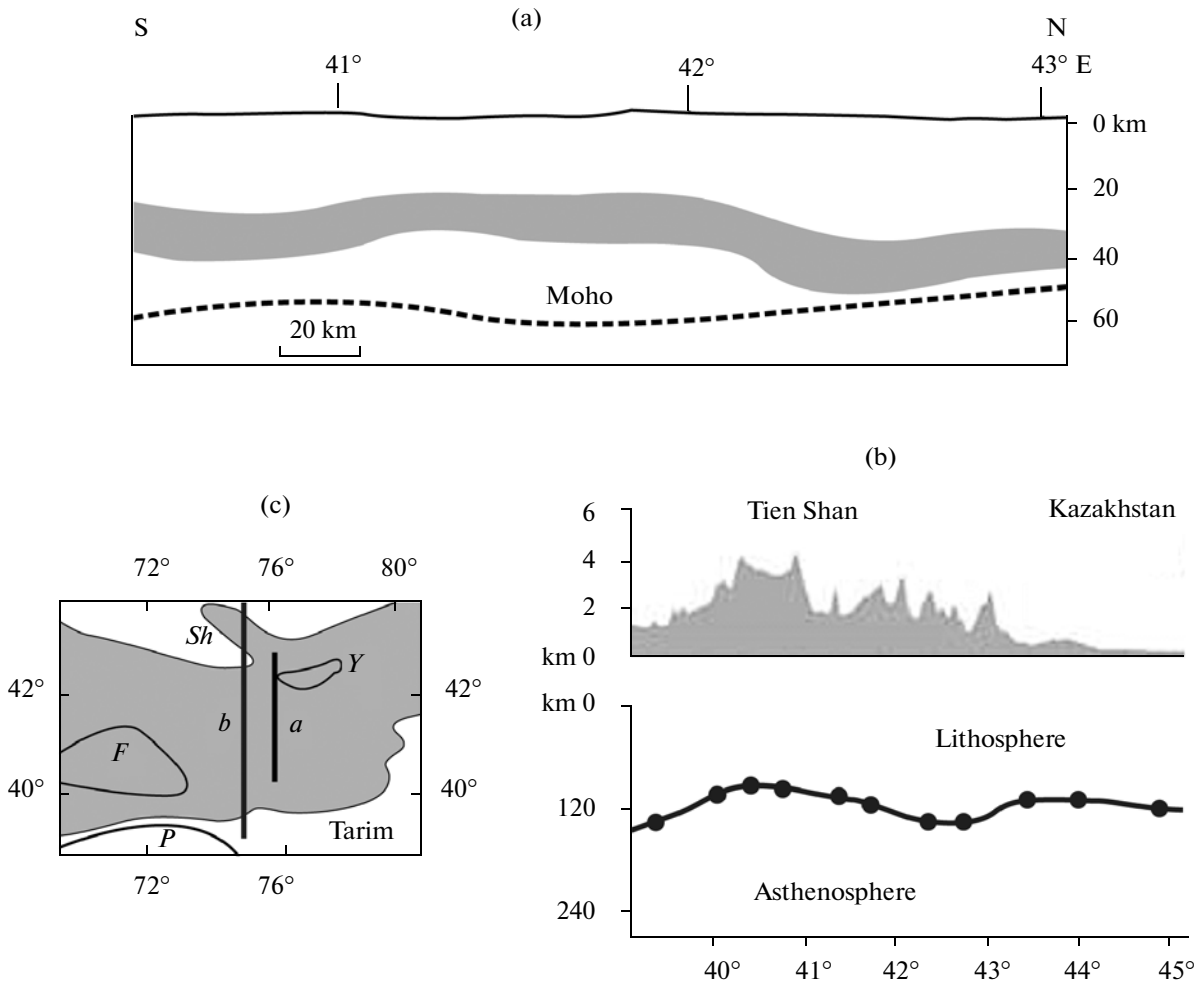

Fig. 12. A waveguide in the Earth's crust and bottom of the lithosphere in the Central Tien Shan inferred from the data of seismic tomography: (a) waveguide (pattern) in the Earth's crust, the Aktüz–Torugart section, after [3]; (b) boundary between lithosphere and asthenosphere beneath the Tien Shan, section along meridian of 75° E, after [61]; the surface topography along the section is shown above (horizontal to vertical scale ratio is 1 : 25); (c) location of seismic lines. *Y*, Lake Ysyk-Köl; *P*, Pamir; *F*, Fergana Basin; *Sh*, Shu Basin; the territory of the Tien Shan is indicated by pattern.

which form unilateral horst-anticlines. The northwestern anticline limbs are upthrown. Owing to the reduced thickness of the Mesozoic–Cenozoic cover, the Paleozoic basement is involved in piedmont deformation in the Keping district. The youngest deformed sediments are lower Miocene in age. A tectonic detachment is suggested in the Cambrian evaporites pertaining to the Paleozoic cover of the Tarim Platform.

In the Kuche sector, the Paleozoic Tien Shan rocks are thrust over the Neogene–Quaternary sediments of the Kuche Basin along a boundary fault. Folding of the Neogene and Pleistocene deposits developed synchronously with sedimentation [95]. It is suggested that steep thrust faults observed at the surface merge at a depth into a low-angle detachment. The petroliferous Kuche Basin has been extensively drilled. Geophysical data and drilling results confirm the thrust deformation style of the Mesozoic and Cenozoic rocks. According to the available information, the holes down to 6 km deep have not reached a detachment. The Kashi–Aksu–Kuche Thrust Fault System strikes in the latitudinal and northeastern directions. The right-lateral Korla Strike-Slip Fault extending in the southeastern direction is conjugated with this system to the east of 85° E. This fault dissects Neogene and older rocks, as well as upper Pleistocene sediments and coeval landforms. Thrust faults and folds in Paleogene and Neogeme rocks are associated with the Korla Strike-Slip Fault. The geological sections based on the principles of thin-skinned tectonics make it possible to estimate their shortening as a result of folding and thrusting: 13–21 km in the Kashi district, 23–25 km in the Keping district (22–28% of the prefolding reconstruction width), and 22–42 km (22–30%) in the Kuche district [57, 95].

The GPS data indicate that the Kashi and Kuche basins are thrusting under the margin of the Eastern Tien Shan with rates of 12.4 ± 0.7 and 5.6 ± 2.1 mm/yr, respectively. The northeastern Tarim is thrust under the Kurugart Range with a rate of 2.9 ± 1.5 mm/yr [91]. The Kashi–Aksu Thrust Fault Zone is shortening with a rate of 8 ± 3 mm/yr [77].

The boundary region between the Central Tien Shan and Tarim is crossed by the Song-Köl–Kashi geophysical transect along the meridian of 76° E (Fig. 7, SK) [19]. The seismic line was shot using the reflection CDP method. The seismological data have been processed as well. As can be seen from the seismic section, a boundary plunges beneath the Tien Shan from the edge of the Tarim Platform (Fig. 11). A high-gradient and low-density zone with displacements of reflectors and decrease in seismic wave velocity within a depth interval of 10 to 45 km corresponds to this boundary. The slope of the boundary surface, which is about 30° in the upper crust, becomes steeper (up to 60°) at a greater depth. Tarim is thrust along this surface under the Tien Shan. The upper crust with a bedded structure is displaced along the zone of continental subduction for 25–40 km. The results of magnetotelluric sounding allow to trace the boundary tectonic zone between the Tien Shan and Tarim below the Moho discontinuity. These and other data show that the boundary between the Tien Shan and Tarim is an underthrust, the surface of which plunges northward, penetrating below the Moho discontinuity. The properties of this zone characterize it as a boundary of secondary lithospheric plates.

The Lithosphere of the Tien Shan

The Earth's crust. According to the seismic and seismological data, the Earth's crust of the Tien Shan has a layered structure. The layers differ from one another in seismic wave velocity, density, and viscosity. The low-velocity layers (waveguides, asthenolayers, asthenolenses) have a lowered viscosity.

As follows from the seismological evidence, the waveguide beneath the Tien Shan is localized at a depth of 20–45 km (Fig. 12). Along the Song-Köl–Kashi seismic line, the waveguide is identified at a depth of 10–20 km (Fig. 11, K1–K2). A similar layer beneath Tarim is thin and detected at a depth of 25–30 km [19]. The decrease in viscosity of the waveguide may be a result of its decompaction (crushing) with pores and fractures filled with fluid; at a depth below 25 km, it may indicate partial melting and migma generation [24]. Many inhomogeneities in the geophysical fields of the upper crust are obliterated beneath the waveguide.

The low-viscosity waveguides exert an appreciable effect on the geodynamics of the crustal processes. The upper boundary of the crustal waveguide is the major geotectonic discontinuity in the Earth's crust. The type and style of deformations change at this level, and disharmony arises between the crustal structure above and below the waveguide. The latter also plays an important role as a layer, the deformation of which isostatically compensates (partly or completely) density heterogeneities in the Earth's crust.

The Moho boundary. In the Tien Shan, the P-wave velocity in the lower crust above the Moho boundary is 6.8–7.4 km/s and 8.0–8.2 km/s immediately below this boundary [19, 24]. The seismic tomographic images from records of earthquakes and nuclear explosions at the Semipalatinsk testing ground show that the depth interval of 35–65 km in the Western and Central Tien Shan has characteristics of a transitional crust–mantle zone. The sharpest change in wave velocity within this zone is interpreted as a bottom of the crust. The P-wave velocities immediately below the Moho boundary are equal to 8.1 km/s at a depth of 35 km beneath the Shu Basin; 7.8–8.0 km/s at a depth of 65 km beneath the Kyrgyz Range; and 7.5 km/s at a depth of 50 km beneath the Ysysk-Köl Basin and surrounding mountain ranges [22, 24].

The average thickness of the Earth's crust of the Tien Shan is ~55 km [87] and 10–15 km greater than in the adjacent territories. In the Western and Central Tien Shan, the Moho boundary occurs at a depth of 40 to 70 km. According to the seismic data (earthquake converted-wave method) the Moho boundary occupies the lowermost position beneath the Kokshaal and Sary-Jaz ranges and rises to a depth of 40 km beneath the Naryn Basin [19, 24]. In the Eastern Tien Shan, the Moho boundary is located at a depth of 50–65 km. The maps of the Moho discontinuity in the Central Tien Shan based on seismological data [87] show that no correlation exists between the topography of the Moho boundary and the Earth's surface of mountain country.

The lithospheric mantle and asthenosphere. The lithosphere of the Central Tien Shan depicted in the seismic section along the meridian of 75° E based on P- and S-wave records has the lowest thickness (90 km) beneath the Torugart Range and the greatest thickness (120 km) beneath the Kyrgyz Range (Fig. 12b). The lithosphere bottom in the southern part of the Eastern Tien Shan is detected at a depth of 200 km and at 150 km in the northern part. The lithosphere bottom beneath the inner parts of the Tarim and Junggar basins is identified at a depth of 250 km [64]. The upper part of the lithospheric mantle, a few kilometers thick, is distinguished by higher seismic wave velocity than the underlying material [87]. In the Central Tien Shan, the seismic tomographic data suggest that collapsed blocks of the continental lithosphere occur in the upper mantle [63].

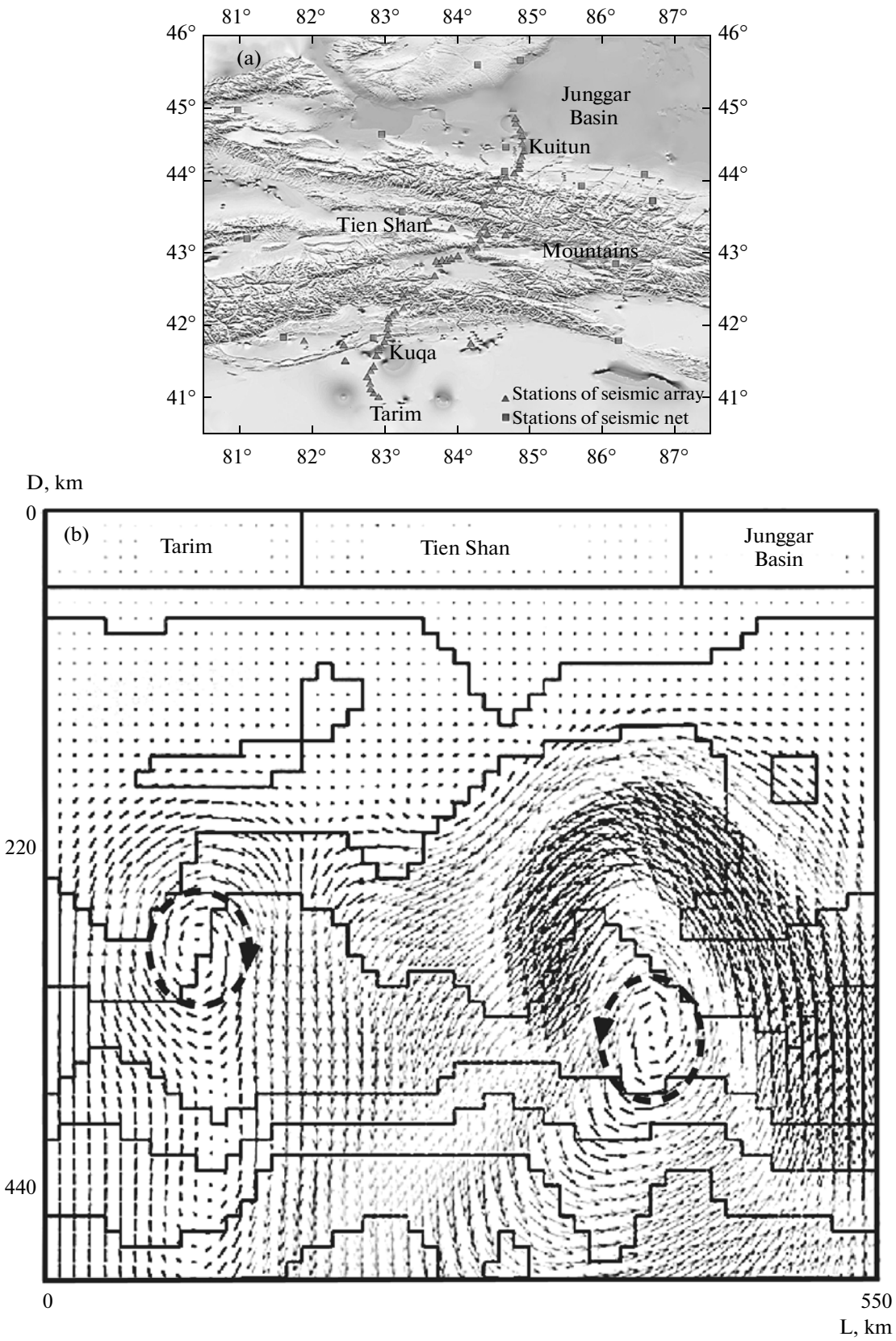

Fig. 13. Convection cells in the upper mantle along the Kuche–Kuitun section across the Eastern Tien Shan, after [64]: (a) location of seismic line and stations; (b) section based on seismic tomographic data; arrows indicate the direction of convection in the mantle. D, depth, km; L, distance along the section, km.

Table 2. Isotopic age of igneous rocks of the Tien Shan

Locality in Fig. 14	No.	Rock	Method	Age, Ma	Source
Kenkol	*1*	Basalt from flow	K-Ar	31–48	[79]
Karakastek	*2*	Basalt from neck	K-Ar	(25 ± 5)*; 46.5	[8]
Suluterek	*3*	Basalt Basalt from flow	K-Ar Ar-Ar	(84 ± 7) 60.5 ± 0.7; 60.7 ± 0.8	[79] [20]
Toruaygyr	*4*	Basalt from sill "	K-Ar Ar-Ar	56 ± 3 53 ± 1	[7] [79]
Uchkuduk	*5*	Limburgite from neck and dikes	K-Ar K-Ar	(21 ± 5); 39 ± 8; 46 ± 2; 51 ± 12 (36 ± 5); 57 ± 9; 63 ± 6	[79] [8]
Tyulek	*6*	Basalt from flow	K-Ar	50 ± 6; 59 ± 2	[79]
Bayduly	*7*	Basalt from flow	K-Ar Ar-Ar	46 ± 10; 53 ± 2 60.6 ± 0.4	[79] [20]
Naryn West	*8*	Limburgite from dikes	K-Ar	99 ± 5; 100 ± 11	[79]
Naryn East	*9*	Basalt	Ar-Ar	52.6 ± 1.2; 54.1 ± 1.2	[79]
Tekelik	*10*	Basalt from flow	K-Ar Ar-Ar	59 ± 2; 74 ± 3 71 ± 3; 74 ± 1; 76 ± 2	[79] [20]
Terek	*11*	Limburgite from dike	K-Ar	61 ± 2	[79]
Toyun	*12*	Lamprophyre, dolerite, and gabbro from sills Basalt from the upper unit Basalt from the lower unit	Ar-Ar K-Ar Ar-Ar K-Ar Ar-Ar Ar-Ar Ar-Ar	46.5 ± 3.8; 59.0 ± 1.4; 67.3 ± 0.1 61.7 ± 3.1 58.5 ± 1.3; 60.4 ± 1.3 101.7 ± 1.1; 113 ± 1.1; 114.2 ± 2.6 104.9 ± 1.1 113.3 ± 1.6; 120 ± 8 112.7 ± 2.3	 [79] [59] [59] [56] [56] [79] [59]
Ming-Kush	*13*	Basalt from flow	K-Ar	68.4 ± 2.3	[4]

Note: Doubtful data are given in parentheses.

The seismic tomography (60 stations) along the Kuche–Kuitun profile, which crosses the Eastern Tien Shan and the adjacent Tarim and Junggar basins (Fig. 13a), provides evidence for the existence of two convection cells in the upper mantle (Fig. 13b). In the Junggar cell, which is outlined beneath the basin bearing the same name and the northern part of the Tien Shan, the convective flow is oriented counterclockwise in section. The rate of this convective flow at the boundary of the upper mantle is higher than 20 mm/yr. The convective flow in the Tarim cell is clockwise in section and weaker than in the Junggar cell. Both flows converge beneath the Southern Tien Shan [64]. Analysis of the gravity field of the Tien Shan also leads to the conclusion about counter convective flows in the upper mantle [38].

Geodynamic Models of the Tien Shan Orogeny

Depending on the authors' views on the main causes of orogeny, the proposed geodynamic models are divided into two groups.

Authigenic orogeny. In terms of the models pertaining to this group, the main cause of orogeny in the Tien Shan is related to the ascent of a mantle plume, decompaction of the lithosphere, influx of fluids, and other local phenomena. The effect of the Hindustan–Eurasia collision is commonly regarded as no more than a complicating factor. Many researchers suggest that all or most of the excess thickness of the present-day thickness of the Earth's crust in the Tien Shan is a result of the ascent of a mantle plume, which gave rise to underplating of the crust. The same plume was also a source of Cretaceous and Paleogene magmatism and a cause of Cenozoic orogeny. It is supposed that the plume's ascent occurred beneath the Central Tien Shan and that its area was comparable with the area of this region or the Tien Shan as a whole [8, 20, 79].

Several arguments cast doubt on the role of the mantle plume in thickening of the crust and the Cenozoic orogeny in the Tien Shan. The magmatic manifestations of the suggested plume activity are tens of million years older than the onset of orogeny (Table 2). In contrast to classic examples, this plume was "lazy." Its magmatic activity lasted for 50–60 Ma with breaks measured in tens of million years. A significant thickness of basalts (up to 300 m) is established only in the small Toyun Syncline in the south of the Central Tien Shan (Fig. 14, locality *12*). The thickness of basalts elsewhere is measured in meters or tens of meters and the area occupied by volcanic flows and sills is no larger than a few kilometers. The amount of magmatic material erupted in the Cretaceous and Paleocene is negligible, whereas the excess volume of the crustal matter in the Tien Shan ascribed to the plume occupies millions of cubic kilometers. For comparison, the plateau basalts of East Siberia related to the mantle plume that erupted during 1 to 8 Ma (from various estimates) are as thick as >3 km and covered 2.5 million square kilometers. The Deccan plateau basalts born by a mantle plume are about 2 km in thickness and spread over one million square kilometers over five million years. The thickness of the Earth's crust in the Tien Shan also argues against the plume model. In the Western Tien Shan (Turkestan–Alay, Zarafshon–Gissar, and Chatkal (Chotkol) mountains), the excess thickness of the crust is as great as in the Central Tien Shan and locally is even greater, but this territory is free of igneous rock occurrences or other evidence for the existence of a mantle plume. All this implies that participation of a vast mantle plume in the formation of the Cretaceous–Paleogene basalts and its contribution to the excess thickness of the present-day crust of the Tien Shan is unlikely.

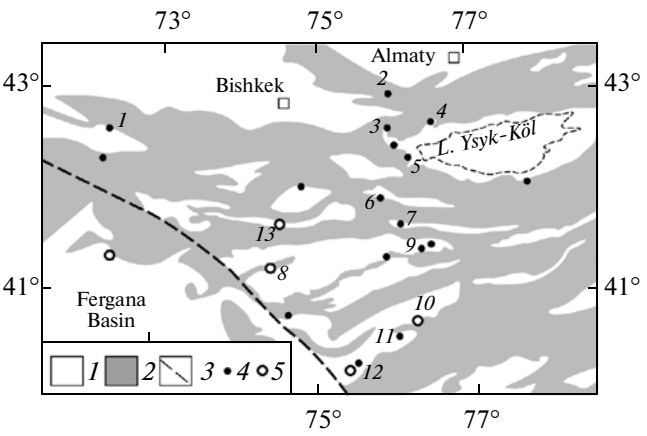

Fig. 14. Occurrences of the Cretaceous and Paleogene magmatic activity in the Central and Western Tien Shan. (*1*) Cenozoic and Mesozoic rocks; (*2*) Paleozoic and pre-Paleozoic rocks; (*3*) Talas–Fergana Fault; (*4, 5*) location of (*4*) Paleogene and (*5*) Cretaceous igneous rocks. See Table 2 for localities *1–13*.

It has also been suggested that mountain building in the Tien Shan is related to local injections of asthenospheric material into the lithosphere and the lower crust beneath mountain ranges [26]. Mountain building continues to the present day, and therefore injections of deep material should inevitably be reflected in the characteristics of heat flow. However, this is not the case. The variation of heat flow, location of the 100°C-isotherm calculated from measurements in drilling holes, and temperature at the Moho surface are not coordinated with the topography of the Tien Shan [17, 24]; therefore, deep injections have little, if any, effect on the orogeny.

The formation of mountain ranges is also explained by outflow of the low-viscous material of the middle crust (waveguide, asthenolayer) from under intermontane basins and by pumping it beneath the ranges [24]. Such a displacement of masses during the orogeny is possible, but this temptingly simple model is not confirmed by seismic data, indicating that thickening of the crust beneath mountain ranges is not a systematic feature.

Allothigenic orogeny. In the models of this group, orogeny in the Tien Shan is considered to be a consequence of interaction between the Tarim, Pamir, Kazakh, and Tien Shan minor (secondary) lithospheric plates, the origin of which and interaction between which is controlled by the Hindustan–Eurasian collision [19, 23, 34, 49, 54, 72]. The boundary zone between the domains differing in strength of the lithosphere is preferential for the appearance of secondary plates. These are the boundaries between the ancient Tarim Craton and the Tien Shan, the Pamirs and Tibet, and between Northern and Central Tibet.

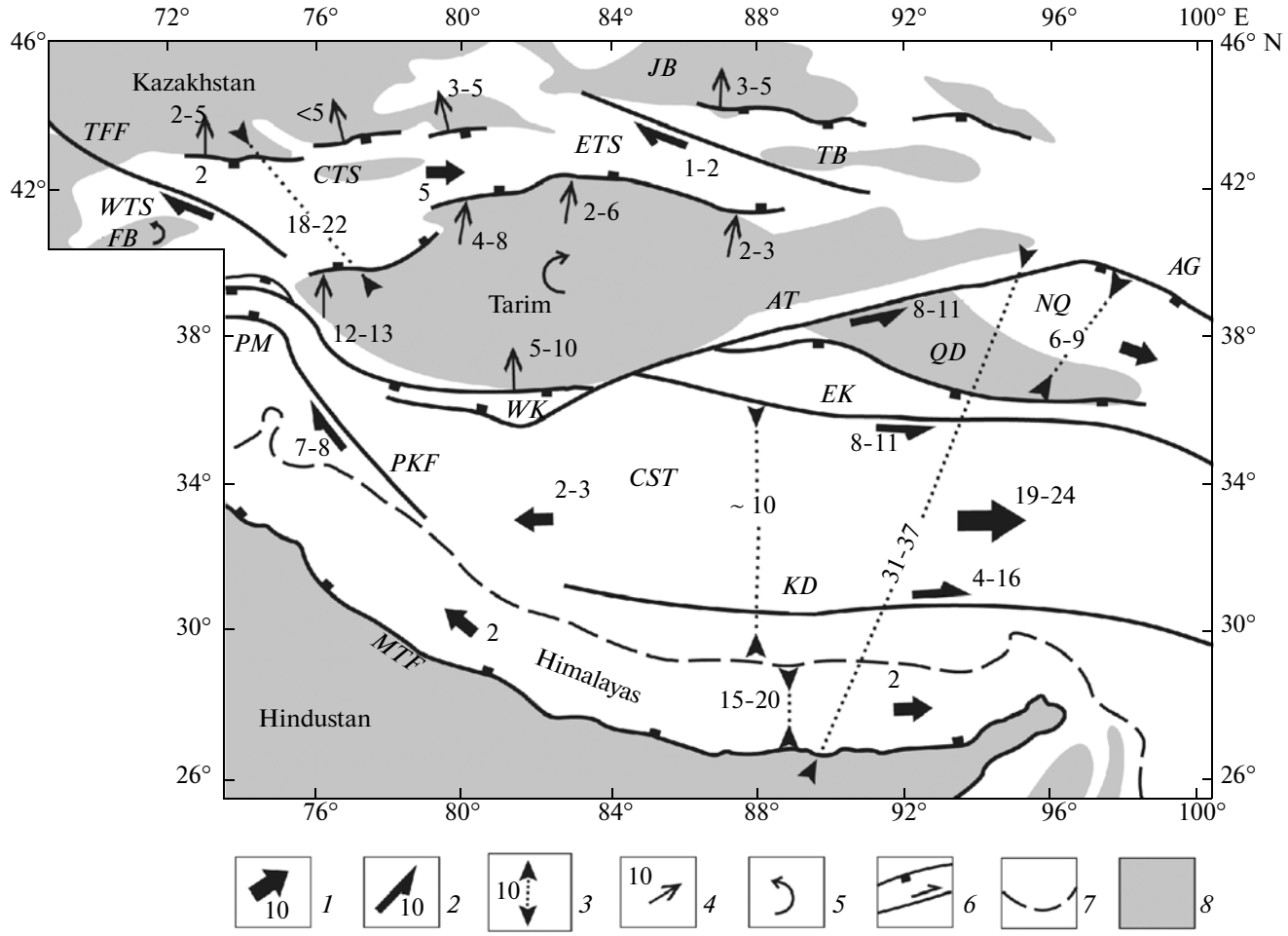

Fig. 15. Contemporary kinematics of interaction between Tibet, Tarim, and Tien Shan. (*1*) Direction of tectonic flow of the Earth's crust and flow rate in the axial zone of flow; (*2*) direction and rate of slip; (*4*) direction and rate of shortening; (*3*) direction and rate of over- or underthrusting; (*5*) direction of sialic block rotation; (*6*) faults; (*7*) Indus–Tsangpo oceanic suture; (*8*) plains and intermontane basins. Flow, displacement, shortening and over- or underthrusting are measured in mm/yr. Structural and morphostructural units (abbreviations in figure): *AG*, Alashan Gobi; *AT*, Altyn Tagh; *EK*, Eastern Kunlun; *ETS*, Eastern Tien Shan; *MTF,* Main Boundary Thrust Fault of the Himalayas; *JB*, Junggar Basin; *WK*, Western Kunlun; *WTS*, Western Tien Shan; *NQ*, Nanshan and Qilianshan; *PKF*, Pamir–Karakoram Fault; *PM*, Pamir; *TB*, Turpan Basin; *TFF*, Talas–Fergana Fault; *FB*, Fergana Basin; *QD*, Qaidam; *CTS,* Central Tien Shan; *CST*, Central and Southern Tibet.

In the models of allothigenic Tien Shan orogeny, Tarim serves as a rigid indentor, which deforms the Central and Eastern Tien Shan. Simulation of interaction between the Tarim and Tien Shan in the Cenozoic has shown that to ensure Cenozoic deformation, the strength of Tarim as an indentor must have been an order of magnitude higher than that of the Tien Shan. Such a difference in strength is realistic. The difference in strength between the ancient Tarim Craton and Paleozoic fold region of the Tien Shan may be either a primary feature or a result of difference in temperature of the lithosphere between them (by 25–30°C at the Moho boundary [73]). A motion transfer from the Hindustan–Eurasia collision zone to the Tien Shan is possible via the lithosphere of Tibet and Tarim, but it seems that a system of convection cells in the mantle is a more probable mechanism.

Geodynamic models of allothigenic orogeny are consistent with the results of geological, geophysical, and geodetic research.

INTERACTION OF TIBET, TARIM, AND THE TIEN SHAN

The contemporary kinematics of interaction between Tibet, Tarim, and the Tien Shan is reflected in displacements along the faults that bound and separate these regions (Fig. 15). The Hindustan Platform is thrust under the Himalayas along the Main Boundary Thrust Fault. Thrusting of Central and Southern Tibet over Tarim (in the Western Kunlun) and Qaidam occurs

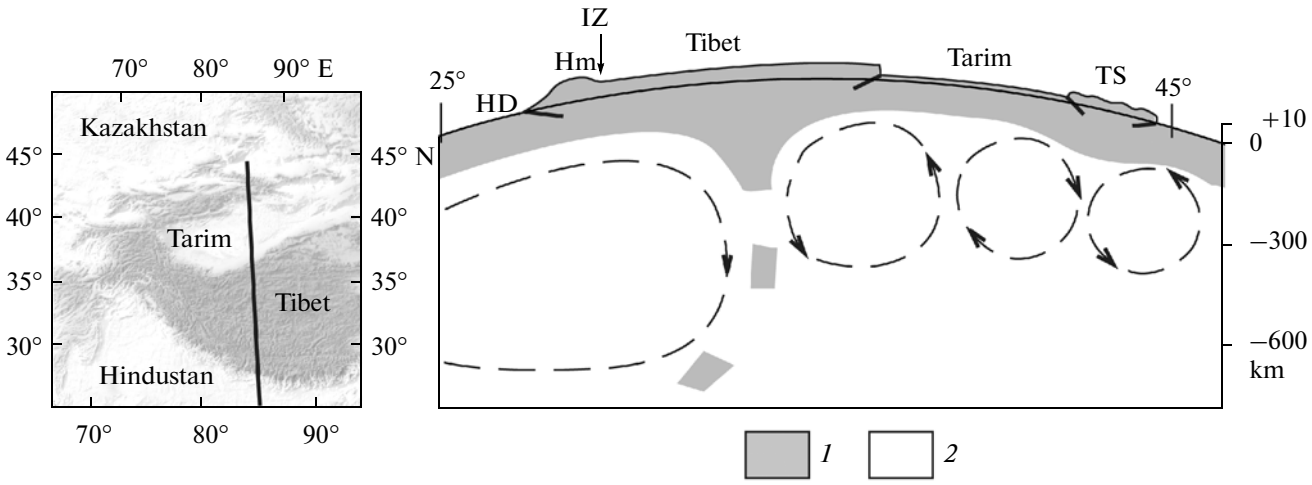

Fig. 16. Geodynamic model of interaction between Hindustan, Tarim, and the Tien Shan in the late Miocene to Quaternary (section along meridian of 85° E). (*1*) Lithosphere, (*2*) athenosphere and C layer of the upper mantle. Abbreviations in figure: Hm, Himalayans; Hd, Hindustan; IZ, Indus–Zangpo Suture; TS, Tien Shan.

at the northern boundary of Central Tibet. In the Western Kunlun, the rate of overthrusting is 5–10 mm/yr. Northern Tibet thrusts over the Alashan Gobi in the Qilianshan and is displaced to the northeast relative to Tarim along the left-lateral Altyn Tagh Strike-Slip Fault.

At the boundary of Tarim with the Central and Eastern Tien Shan, the Kashi Basin is thrust under the margin of the Central Tien Shan with a rate of 12–13 mm/yr, and the Kuche Basin is thrust under the margin of the Eastern Tien Shan with a rate of 4–8 mm/yr. Interpretation of the GPS data indicates that the Tarim Block rotates clockwise relative to the stable Eurasia with an angular rate of 0.52°/Ma [91]. At the northern boundary of the Central Tien Shan, the Kyrgyz Range thrusts over the Shu Basin with a rate of 2–5 mm/yr; the Transili Range thrusts over the Ili basin with a rate of ~5 mm/yr; and the Ketmen Range thrusts over the same basin with a rate of 3–5 mm/yr. The Junggar Tien Shan thrusts over the basin bearing the same name with a rate of 3–5 mm/yr.

The general deformation of the region gives rise to the schortening of its area in the nearly meridional direction. The rate of transverse shortening of Tibet is more than 30 mm/yr. To a great extent, this shortening is compensated by squeezing-out of the crust into a geodynamic refuge to the east and southeast of Tibet. The rate of tectonic flow in Central Tibet exceeds 20 mm/yr. The transverse shortening of the Tien Shan develops with almost the same average rate. The shortening is compensated by boundary and internal deformations and partly by eastward tectonic flow with a rate reaching 5 mm/yr.

The proposed geodynamic model of interaction between Hindustan, Tibet, Tarim, and the Tien Shan demonstrates a mechanism of motion transfer from the Hindustan–Eurasia convergence zone to Tarim and the Tien Shan (Fig. 16). The model is based on the data considered above and their interpretation. The most important information has been obtained as a result of sesimic tomography, seismological study, and seismic profiling. Taken together, these data provide evidence for (i) the existence of convection cells in the upper mantle beneath the Tien Shan and Tarim and their dimensions; (ii) the scale and limits of underthrusting (subduction) of the Hindustan continental lithosphere beneath Tibet; (iii) thrusting of Tarim and North Tibet under Central Tibet; and (iv) underthrusting of Tarim beneath the Central and Eastern Tien Shan.

ACKNOWLEDGMENTS

I thank N.V. Koronovsky, T.V. Romanyuk, and V.G. Trifonov for their helpful reviews and constructive comments.

REFERENCES

1. K. E. Abdrakhmatov, R. Weldon, S. Thompson, D. Burbank, Ch. Rubin, M. Miller, and P. Molnar, "Onset, Style, and Current Rate of Shortening in the Central Tien Shan," Geol. Geofiz. **42**, 1585–1609 (2001).
2. Z. V. Aleshinskaya, T. N. Voskresenskaya, O. A. Kulikov, and S. S. Faustov, "Stratigraphic Position of the Sharpyldag Formation in the Light of Paleomagnetic Data," Vestnik MGU, Ser. Geogr., No. 5, 106–107 (1972).
3. A. B. Bakirov, O. M. Lesik, A. P. Lobanchenko, and T. M. Sabitova, "Signs of Contemporary Deep Magmatism in the Tien Shan," Geol. Geofiz. **37** (12), 42–53 (1996).

4. D. M. Bachmanov, V. G. Trifonov, A. V. Mikolaichuk, F. A. Vishnyakov, and A. A. Zarshchikov, "The Ming-Kush-Kokomeren Zone of Recent Transpression in the Middle Tien Shan," Geotectonics **42** (3), 186–205 (2008). doi: 10.1134/S0016853X0803003X
5. V. S. Burtman, "Tectonic Flow in the Alpine Belt," Izv. Akad. Nauk SSSR, Ser. Geol., No. 6, 30–39 (1990).
6. V. S. Burtman, "Tien Shan, Pamir, and Tibet: History and Geodynamics of Phanerozoic Oceanic Basins," Geotectonics **44** (3), 388–404 (2010). doi: 10.1134/S001685211005002X
7. L. K. Gabuniya, E. V. Devyatkin, and M. M. Rubinstein, "Absolute Age of the Cenozoic Continental Sedimentary Rocks of Asia and Its Biostratigraphic Implications," Dokl. USSR Acad. Sci. **225**, 895–898 (1975).
8. A. F. Grachev, "Early Cenozoic Magmatism and Geodynamics of North Tien Shan," Izv. Physics Solid Earth **35** (10), 815–839 (1999).
9. O. M. Grigina and A. B. Fortuna, *Paleogeography of the North Tien Shan in Cenozoic* (Ilim, Frunze, 1981) [in Russian].
10. N. L. Dobretsov, A. G. Kirdyashkin, and A. A. Kirdyashkin, *Deep Geodynamics* (Siberian Branch, RAS, Novosibirsk, 2001) [in Russian].
11. A. V. Zubovich, V. I. Makarov, S. I. Kuzikov, O. I. Mosienko, and G. G. Shchelochkov, "Intracontinental Mountain Building in Central Asia As Inferred from Satellite Geodetic Data," Geotectonics **41** (1), 13–25 (2007). doi: 10.1134/S0016853X07010031
12. A. V. Zubovich and O. I. Mosienko, "Distribution of Recent Deformations in the Tien Shan Region," in *Geodynamics and Environmental Problems of High-Mountain Regions* (Bild, Bishkek, 2002), pp. 105–107 [in Russian].
13. *The Neotectonic Map of Northern Eurasia on a Scale of 1 : 5000000*, Ed. by G. F. Grachev (OIFZ RAN, Moscow, 1997) [in Russian].
14. M. L. Kopp, *Structures of Lateral Extrusion in the Alpine–Himalayan Collision Belt* (Nauchnyi mir, Moscow, 1997) [in Russian].
15. A. M. Korjenkov and A. V. Mikolaichuk, "Mesozoic–Cenozoic Intracontinental and Orogenic Complexes and Neotectonics," in *Tectonic Evolution and Structure of the Earth's Crust of the Tien Shan and Adjacent Regions: Guidebook of Excursion* (Geol. Inst. Nat. Acad. Sci., Bishkek, 2009), pp. 68–80 [in Russian].
16. M. G. Leonov, *Tectonics of the Consolidated Crust* (Nauka, Moscow, 2008) [in Russian].
17. *Lithosphere of the Tien Shan*, Ed. by I. E. Gubin (Nauka, Moscow, 1986) [in Russian].
18. V. I. Makarov, *Neotectonic Structure of the Central Tien Shan* (Nauka, Moscow, 1977) [in Russian].
19. V. I. Makarov, D. V. Alekseev, V. Yu. Batalev, et al., "Underthrusting of Tarim beneath the Tien Shan and Deep Structure of Their Junction Zone: Main Results of Seismic Experiment along MANAS Profile Kashgar-Song-Kol," Geotectonics **44** (2), 102–126 (2010). doi: 10.1134/S0016853X10020025
20. A. V. Mikolaichuk, V. A. Simonov, A. I. Travin, and E. R. Sobel, "Mesozoic and Cenozoic Plume Magmatism of the Central Tien Shan," in *Geodynamics and Ecology of High-Mountain Regions in the 21st Century*, Ed. by. M. G. Leonov (Moscow–Bishkek, 2006), Issue 1, pp. 50–57 [in Russian].
21. *Neotectonics, Geodynamics, and Seismicity of Northern Eurasia,* Ed. by A. F. Grachev (Probel, Moscow, 2000) [in Russian].
22. T. M. Sabitova and A. A. Adamova, "Seismic Tomographic Studies of the Earth's Crust in the Tien Shan," Geol. Geofiz. **42**, 1543–1553 (2001).
23. I. Sadybakasov, *Neotectonics of High Asia* (Nauka, Moscow, 1990) [in Russian].
24. *Recent Geodynamics of the Regions of Intracontinental Collision Mountain Building*, Ed. by V. I. Makarov, (Nauchnyi mir, Moscow, 2005) [in Russian].
25. N. A. Sycheva, S. L. Yunga, L. M. Bogomolov, and V. I. Makarov, "Seismotectonic Deformations and Recent Tectonics of the Tien Shan," Physics Solid Earth **44** (5), 351–363 (2008).
26. V. G. Trifonov, E. V. Artyushkov, A. E. Dodonov, D. M. Bachmanov, A. V. Mikolaichuk, and F. A. Vishnyakov, "Pliocene–Quaternary Mountain Building in the Central Tien Shan," Geol. Geofiz. **49** (2), 128–145 (2008).
27. V. I. Ulomov, *Dynamics of the Earth's Crust in Central Asia and Prediction of Earthquakes* (Fan, Tashkent, 1974) [in Russian].
28. O. K. Chediya, *Morphostructures and Recent Tectogenesis of the Tien Shan* (Ilim, Frunze, 1986) [in Russian].
29. S. S. Schultz, *Analysis of Neotectonics and Topography in the Tien Shan* (Geografgiz, Moscow, 1948) [in Russian].
30. J. C. Aitchison, J. R. Ali, and A. M. Davis, "When and Where Did India and Asia Collide?" J. Geophys. Res. **112** (B05423), 1–19 (2007).
31. M. B. Allen, B. F. Windley, and C. Zhang, "Cenozoic Tectonics of the Urumqi–Korla Region of the Chinese Tien Shan," Geol. Rundsh. **83**, 406–416 (1994).
32. E. Argand, "La Tectonique de l'Asie," in *Proc. 13th Intern. Geol. Congr. (1922)* (Brussels, 1924), Vol. 1, Pt. 5, pp. 170–372.
33. R. Armijo, P. Tapponnier, and T. Han, "Late Cenozoic Right-Lateral Strike-Slip Faulting in Southern Tibet," J. Geophys. Res. 1989, **94**, 2787–2838 (1989).
34. J. P. Avouac and P. Tapponnier, "Kinematic Model of Active Deformation in Central Asia," J. Geophys. Res. Lett. **20**, 895–898 (1993).
35. C. Braitenberg, M. Zadro, J. Fang, Y. Wang, and H. T. Hsu, "The Gravity and Isostatic Moho Undulations in Qinghai–Tibet Plateau," J. Geodynamics **30**, 489–505 (2000).
36. M. E. Bullen, D. W. Burbank, J. I. Garver, and K. Y. Abdrakhmatov, "Late Cenozoic Tectonic Evolution of the Northwestern Tien Shan: New Age Estimates for the Initiation of Mountain Building," Geol. Soc. Amer. Bull. **113**, 1544–1559 (2001).
37. M. E. Bullen, D. W. Burbank, and J. I. Garver, "Building the Northern Tien Shan: Integrated Thermal, Structural, and Topographic Constraints," J. Geol. **111**, 149–165 (2003).

38. E. V. Burov, M. G. Kogan, H. Lyon-Caen, and P. Molnar, "Gravity Anomalies, the Deep Structure, and Dynamic Processes beneath the Tien Shan," Earth Planet. Sci. Lett. **96**, 367–383 (1990).

39. V. S. Burtman, S. F. Scobelev, and P. Molnar, "Late Cenozoic Slip on the Talas-Ferghana Fault, Tien Shan, Central Asia," Geol. Soc. Amer. Bull. **108**, 1004–1021 (1996).

40. C. Chang, *Geology and Tectonics of the Qinghai–Tibet Plateau* (Science Press, Beijing, 1996).

41. J. Charreau, J.-P. Avouac, Y. Chen, S. Dominguez, and S. Gilder, "Miocene to Present Kinematics of Fault-Bend Folding across the Huerguosi Anticline, Northern Tianshan (China), Derived from Structural, Seismic, and Magnetostratigraphic Data," Geology **36**, 871–874 (2008).

42. J. Charreau, S. Gilder, Y. Chen, S. Dominguez, J.-P. Avouac, S. Sevket, M. Jolivet, Y. Li, and W. Wang, "Magnetostratigraphy of the Yaha Section, Tarim Basin (China): 11 Ma Acceleration in Erosion and Uplift of the Tian Shan Mountains," Geology **34**, 181–184 (2006).

43. J. Chen, R. Heermance, and D. W. Burbank, K. M. Scharer, J. Miao, and C. Wang, "Quantification of Growth and Lateral Propagation of the Kashi Anticline, Southwest Chinese Tian Shan," J. Geophys. Res. **112** (B03S16) 1–22 (2007).

44. Q. Chen, J. T. Freymueller, Q. Wang, Z. Yang, C. Xu, and J. Liu, "A Deforming Block Model for the Present-Day Tectonics of Tibet," J. Geophys. Res. **109** (B01403), 1–16 (2004).

45. W. Chen, M. Martin, T. Tseng, R. L. Nowack, S. Hung, and B. Huang, "Shear-Wave Birefringence and Current Configuration of Converging Lithosphere under Tibet," Earth Planet. Sci. Lett. **295**, 297–304 (2010).

46. M. P. Coward and R. W. H. Butler, "Thrust Tectonics and the Deep Structure of the Pakistan Himalaya," Geology **13**, 417–420 (1985).

47. E. Cowgill, R. D. Gold, X. Chen, X. Wang, J. R. Arrowsmith, and J. Southon, "Low Quaternary Slip Rate Reconciles Geodetic and Geologic Rates along the Altyn Tagh Fault, Northwestern Tibet," Geology **37**, 647–650 (2009).

48. P. G. DeCelles, D. M. Robinson, and G. Zandt, "Implications of Shortening in the Himalayan Fold-Thrust Belt for Uplift of the Tibetan Plateau," Tectonics **21** (1062), 1–25 (2002).

49. J. DeGrave, M. M. Buslov, and P. Vandenhaute, "Distant Effects of India–Eurasia Convergence and Mesozoic Intracontinental Deformation in Central Asia: Constraints from Apatite Fission-Track Thermochronology," J. Asian Earth Sci. **29**, 188–204 (2007).

50. L. Ding, P. Kapp, and X. Wan, "Paleocene–Eocene Record of Ophiolite Obduction and Initial India–Asia Collision, South Central Tibet," Tectonics **24** (TC3001), 1–18 (2005).

51. G. Dupont-Nivet, B. K. Horton, R. F. Butler, J. Wang, J. Zhou, and G. L. Waanders, "Paleogene Clockwise Tectonic Rotation of the Xining–Lanzhou Region, Northeastern Tibetan Plateau," J. Geophys. Res. **109** (B04401), 1–13 (2004).

52. G. Dupont-Nivet, P. C. Lippert, D. J. Hinsbergen, M. J. Meijers, and P. Kapp, "Palaeolatitude and Age of the Indo-Asia Collision: Palaeomagnetic Constraints," Geophys. J. Int. **182**, 1189–1198 (2010).

53. B. Fu and Y. Awata, "Displacement and Timing of Left-Lateral Faulting in the Kunlun Fault Zone, Northern Tibet, Inferred from Geologic and Geomorphic Features," J. Asian Earth Sci. **29**, 253–265 (2007).

54. B. Fu, A. Lin, K. Kano, T. Maruyama, and J. Guo, "Quaternary Folding of the Eastern Tian Shan, Northwest China," Tectonophysics **369**, 79–101 (2003).

55. R. Gao, Z. Lu, Q. Li, Y. Guan, J. Zhang, R. He, and L. Huang, "Geophysical Survey and Geodynamic Study of Crust and Upper Mantle in the Qinghai–Tibet Plateau," Episodes **28**, 263–273 (2005).

56. B. Han, X. Wang, G. He, N. Wu, M. Li, Y. Liu, and S. Wang, "Discovery of Mantle and Lower Crust Xenoliths from Early Cretaceous Volcanic Rocks of Southwestern Tianshan, Hinjiang," Chinese Sci. Bull. **44**, 1119–1122 (1999).

57. R. V. Heermance, V. Richard, J. Chen, D. W. Burbank, W. Douglas, and C. Wang, "Chronology and Tectonic Controls of Late Tertiary Deposition in the Southwestern Tian Shan Foreland, NW China," Basin Res. **19**, 599–632 (2007).

58. B. Huang, J. D. A. Piper, S. Peng, T. Liu, Z. Li, Q. Wang, and R. Zhu, "Magnetostratigraphic Study of the Kuche Depression, Tarim Basin, and Cenozoic Uplift of the Tian Shan Range, Western China," Earth Planet. Sci. Lett. **251**, 346–364 (2006).

59. B. Huang, J. D. A. Piper, Y. Wang, H. He, and R. Zhu, "Paleomagnetic and Geochronological Constraints on the Post-Collisional Northward Convergence of the Southwest Tian Shan, NW China," Tectonophysics **409**, 107–124 (2005).

60. G. Kosarev, R. Kind, S. V. Sobolev, X. Yuan, W. Hanka, and S. Oreshin, "Seismic Evidence for a Detached Indian Lithospheric Mantle beneath Tibet," Science **283**, 1306–1309 (1999).

61. P. Kumar, X. Yuan, R. Kind, and G. Kozarev, "The Lithosphere–Asthenosphere Boundary in the Tien Shan–Karakoram Region from S Receiver Functions: Evidence for Continental Subduction," Geophys. Res. Lett. **32** (L07305), 1–4 (2005).

62. P. Kumar, X. Yuan, R. Kind, and J. Ni, "Imaging the Colliding Indian and Asian Lithospheric Plates Beneath Tibet," J. Geophys. Res. **111**, 6308–6319 (2006).

63. Z. W. Li, S. Roecker, Z. H. Li, B. Wei, H. Wang, G. Schelochkov, and V. Bragin, "Tomographic Image of the Crust and Upper Mantle beneath the Western Tien Shan from the MANAS Broadband Deployment: Possible Evidence for Lithospheric Delamination," Tectonophysics **477**, 49–57 (2009).

64. J. Liu, Q. Liu, B. Guo, D. A. Yuen, and H. Song, "Small-Scale Convection in the Upper Mantle beneath the Chinese Tian Shan Mountains," Phys. Earth Planet. Inter. **163**, 179–190 (2007).

65. M. Liu and Y. Yang, "Extensional Collapse of the Tibetan Plateau: Results of Three-Dimensional Finite

Element Modeling," J. Geophys. Res. **108** (B2361), 1–15 (2003).

66. X. Ma, *Litospheric Dynamic Map of China and Adjacent Seas on a Scale 1 : 4000000* (Geol. Publ. House, Beijing, 1987).
67. P. Matte, P. Tapponnier, N. Arnaud, L. Bourjot, J. P. Avouac, P. Vidal, Q. Liu, Y. Pan, and Y. Wang, "Tectonics of Western Tibet between the Tarim and the Indus," Earth Planet. Sci. Lett. **142**, 311–330 (1996).
68. P. Molnar, P. England, and J. Martinod, "Mantle Dynamics, Uplift of the Tibetan Plateau, and the Indian Monsoon," Rev. Geophys. **31**, 357–396 (1993).
69. P. Molnar and S. Ghose, "Seismic Moments of Major Earthquakes and the Rate of Shortening across the Tien Shan," Geophys. Res. Lett. **27**, 2377–2380 (2000).
70. P. Molnar and H. Lyon-Caen, "Fault Plane Solutions of Earthquakes and Active Tectonics of the Tibetan Plateau and Its Margins," Geophys. J. Int. **99**, 123–153 (1989).
71. P. Molnar and M. Stock, "Slowing of India's Convergence with Eurasia since 20 Ma and Its Implications for Tibetan Mantle Dynamics," Tectonics **28**, 3001–3011 (2009).
72. P. Molnar and P. Tapponnier, "Cenozoic Tectonics of Asia: Effects of a Continental Collision," Science **169**, 419–426 (1975).
73. A. Neil and G. A. Houseman, "Geodynamics of the Tarim Basin and the Tian Shan in Central Asia," Tectonics **16**, 571–584 (1997).
74. S. Nomade, P. R. Renne, X. Mo, Z. Zhao, and S. Zhou, "Miocene Volcanism in the Lhasa Block, Tibet: Spatial Trends and Geodynamic Implications," Earth Planet. Sci. Lett. **221**, 227–243 (2004).
75. C. Powell, "Continental Underplating Model for the Rise of the Tibetan Plateau," Earth Planet. Sci. Lett. **81**, 79–94 (1986/1987).
76. L. Ratschbacher, W. Frisch, U. Herrman, and M. Strecker, "Distributed Deformation in Southern and Western Tibet during and after the India–Asia Collision: An Experimental Approach," J. Geophys. Res. **99**, 19917–19945 (1994).
77. C. Reigber, G. W. Michel, R. Galas, D. Angermann, J. Klotz, J. Y. Chen, A. Papschev, R. Arslanov, V. E. Tzurkov, and M. C. Ishanov, "New Space Geodetic Constraints on the Distribution of Deformation in Central Asia," Earth Planet. Sci. Lett. **191**, 157–165 (2001).
78. D. B. Rowley, "Age of Initiation of Collision between India and Asia: A Review of Stratigraphic Data," Earth Planet. Sci. Lett. **145**, 1–13 (1996).
79. E. R. Sobel and N. Arnaud, "Cretaceous–Paleogene Basaltic Rocks of the Tuyon Basin, NW China and the Kyrgyz Tian Shan: The Trace of a Small Plume," Lithos **50**, 191–215 (2000).
80. E. R. Sobel, J. Chen, and R. V. Heermance, "Late Oligocene–Early Miocene Initiation of Shortening in the Southwestern Chinese Tian Shan: Implications for Neogene Shortening Rate Variations," Earth Planet. Sci. Lett. **247**, 70–81 (2006).
81. E. R. Sobel and T. A. Dumitru, "Thrusting and Exhumation around the Margins of the Western Tarim Basin during the India–Asia Collision," J. Geophys. Res. **102**, 5043–5064 (1997).
82. J. Sun and Z. Zhang, "Syntectonic Growth Strata and Implications for Late Cenozoic Tectonic Uplift in the Northern Tian Shan, China," Tectonophysics **463**, 60–68 (2009).
83. J. Sun, R. Zhu, and J. Bowler, "Timing of the Tianshan Mountains Uplift Constrained by Magnetostratigraphic Analysis of Molasse Deposits," Earth Planet. Sci. Lett. **219**, 239–253 (2004).
84. P. Tapponnier, F. J. Ryerson, J. Woerd, A. Mriaux, and C. Lasserre, "Long-Term Slip Rates and Characteristic Slip: Keys to Active Fault Behaviour and Earthquake Hazard," Earth Planet. Sci. Lett. **333**, 483–494 (2001).
85. M. Taylor and A. Yin, "Active Structures of the Himalayan–Tibetan Orogen and Their Relationships to Earthquake Distribution, Contemporary Strain Field, and Cenozoic Volcanism," Geosphere **5**, 199–214 (2009).
86. S. C. Thompson, R. J. Weldon, C. M. Rubin, K. Abdrakhmatov, P. Molnar, and G. W. Berger, "Late Quaternary Slip Rates across the Central Tien Shan, Kyrgyzstan, Central Asia," J. Geophys. Res. **107** (B2203), 1–32 (2002).
87. L. P. Vinnik, C. Reigber, I. M. Aleshin, G. L. Kosarev, V. K. Kaban, S. L. Oreshin, and S. W. Roecker, "Receiver Function Tomography of the Central Tien Shan," Earth Planet. Sci. Lett. **225**, 131–146 (2004).
88. C. Wang, X. Zhao, Z. Liu, P. C. Lippert, S. A. Graham, R. S. Coe, H. Yi, L. Zhu, S. Liu, and Y. Li, "Constraints on the Early Uplift History of the Tibetan Plateau," Proceeding Nat. Acad. Sci. USA **105**, 4987–4992 (2008).
89. G. Wittlinger, J. Vergne, P. Tapponnier, V. Farra, G. Poupinet, M. Jiang, H. Su, G. Herquel, and A. Paul, "Teleseismic Imaging of Subducting Lithosphere and Moho Offsets beneath Western Tibet," Earth Planet. Sci. Lett. **221**, 117–130 (2004).
90. L. Xia, X. Li, Z. Ma, X. Xu, and Z. Xia, "Cenozoic Volcanism and Tectonic Evolution of the Tibetan Plateau," Gondwana Res. **19**, 850–866 (2010).
91. S. Yang, J. Li, and Q. Wang, "The Deformation Pattern and Fault Rate in the Tianshan Mountains Inferred from GPS Observations," Science in China, Ser. D, Earth Sci. **51**, 1064–1080 (2008).
92. A. Yin, "Mode of Cenozoic East–West Extension in Tibet Suggesting a Common Origin of Rifts in Asia during the Indo-Asian Collision," J. Geophys. Res. **105**, 21745–21759 (2000).
93. A. Yin, "Cenozoic Tectonic Evolution of the Himalayan Orogen as Constrained by Along-Strike Variation of Structural Geometry, Exhumation History, and Foreland Sedimentation," Earth-Sci. Rev. **76**, 1–131 (2006).
94. A. Yin and T. M. Harrison, "Geological Evolution of the Himalayan–Tibetan Orogen," Ann. Rev. Earth Planet. Sci. **28**, 211–280 (2000).
95. A. Yin, S. Nie, P. Craig, T. M. Harrison, F. J. Ruerson, Q. Xianglin, and Y. Geng, "Late Cenozoic Evolution

of the Southern Chinese Tian Shan," Tectonics **17**, 1–27 (1998).

96. Y. Yue, B. D. Ritts, and S. A. Graham, "Initiation and Long-Term Slip History of the Altyn Tagh Fault," Int. Geol. Rev. **43**, 1087–1093 (2001).
97. P. Zhang, P. Molnar, and X. Xu, "Late Quaternary and Present-Day Rates of Slip along the Altyn Tagh Fault, Northern Margin of the Tibetan Plateau," Tectonics **26** (TC5010), 1–24 (2007).
98. P. Zhang, Z. Shen, M. Wang, W. Gan, R. Bürgmann, P. Molnar, Q. Wang, Z. Niu, J. Sun, J. Wu, H. Sun, and X. You, "Continuous Deformation of the Tibetan Plateau from Global Positioning System Data," Geology **32**, 809–812 (2004).
99. J. Zhao, X. Yuan, H. Liu, P. Kumar, S. Pei, R. Kind, Z. Zhang, J. Tenge, L. Dinga, X. Gao, Q. Xua, and W. Wanga, "The Boundary between the Indian and Asian Tectonic Plates Below Tibet," Proceedings National Academy Sci. USA **107**, 11229–11233 (2010).
100. Z. Zhao, X. Mo, Y. Dilek, Y. Niu, D. J. DePaolo, P. Robinson, D. Zhu, C. Sun, G. Dong, S. Zhou, Z. Lui, and Z. Hou, "Geohemical and Sr–Nd–Pb–O Isotopic Compositions of the Post-Collisional Ultrapotassic Magmatism in SW Tibet: Petrogenesis and Implications for India Intracontinental Subduction beneath Southern Tibet," Lithos **113**, 190–212 (2009).
101. F. V. Zubovich, X. Wang, Y. G. Scherba, et al., "GPS Velocity Field for the Tien Shan and Surrounding Regions," Tectonics **29** (TS6014), 1–23 (2010).

Reviewers: N.V. Koronovsky, T.V. Romanyuk, and V.G. Trifonov